

AB INITIO DESIGN OF NOVEL MAGNESIUM ALLOYS FOR
HYDROGEN STORAGE

A THESIS SUBMITTED TO
THE GRADUATE SCHOOL OF NATURAL AND APPLIED SCIENCES
OF
MIDDLE EAST TECHNICAL UNIVERSITY

BY

DENİZ KEÇİK

IN PARTIAL FULFILLMENT OF THE REQUIREMENTS
FOR
THE DEGREE OF MASTER OF SCIENCE
IN
METALLURGICAL AND MATERIALS ENGINEERING

JULY 2008

Approval of the thesis:

**AB INITIO DESIGN OF NOVEL MAGNESIUM ALLOYS FOR
HYDROGEN STORAGE**

submitted by **DENİZ KEÇİK** in partial fulfillment of the requirements for the degree of **Master of Science in Metallurgical and Materials Engineering, Middle East Technical University** by

Prof.Dr. Canan Özgen
Dean, Graduate School of **Natural and Applied Sciences** _____

Prof.Dr. Tayfur Öztürk
Head of Department, **Metallurgical and Materials Engineering** _____

Prof.Dr. M. Kadri Aydınol
Supervisor, **Metallurgical and Materials Engineering Dept., METU** _____

Examining Committee Members:

Prof.Dr. Tayfur Öztürk
Metallurgical and Materials Engineering Dept., METU _____

Prof.Dr. M. Kadri Aydınol
Metallurgical and Materials Engineering Dept., METU _____

Prof.Dr. Şakir Bor
Metallurgical and Materials Engineering Dept., METU _____

Assist. Prof.Dr. Arcan Dericioğlu
Metallurgical and Materials Engineering Dept., METU _____

Assist. Prof.Dr. Zafer Evis
Engineering Sciences Dept., METU _____

Date: _____ 31.07.2008

I hereby declare that all information in this document has been obtained and presented in accordance with academic rules and ethical conduct. I also declare that, as required by these rules and conduct, I have fully cited and referenced all material and results that are not original to this work.

Name, Last Name : Deniz Keçik

Signature :

ABSTRACT

AB INITIO DESIGN OF NOVEL MAGNESIUM ALLOYS FOR HYDROGEN STORAGE

Keçik, Deniz

M.S., Department of Metallurgical and Materials Engineering

Supervisor: Prof. Dr. M. Kadri Aydınol

July 2008, 66 pages

A candidate hydrogen storing material should have high storage capacity and fast dehydrogenation kinetics. On this basis, magnesium hydride (MgH_2) is an outstanding compound with 7.66 wt % storage capacity, despite its slow dehydrating kinetics and high desorption temperature. Therefore in this study, bulk and surface alloys of Mg with improved hydrogen desorption characteristics were investigated. In this respect, formation energies of alloyed bulk MgH_2 as well as the adsorption energies on alloyed magnesium (Mg) and MgH_2 surface structures were calculated by total energy pseudopotential methods. Furthermore, the effect of substitutionally placed dopants on the dissociation of hydrogen molecule (H_2) at the surface of Mg was studied via Molecular Dynamics (MD). The results displayed that 31 out of 32 selected dopants contributed to the decrease in formation energy of MgH_2 within a range of ~ 37 kJ/mol- H_2 where only Sr did not exhibit any such effect. The most favorable elements in this respect came out to be; P, K, Tl, Si, Sn, Ag, Pb, Au, Na,

Mo, Ge and In. Afterwards, a systematical study within adsorption characteristics of hydrogen on alloyed Mg surfaces (via dynamic calculations) as well as calculations regarding adsorption energies of the impurity elements were performed. Accordingly, Mo and Ni yielded lower adsorption energies; -9.2626 and -5.2995 eV for substitutionally alloyed surfaces, respectively. MD simulations presented that Co is found to have a splitting effect on H₂ in 50 fs, where the first hydrogen atom is immediately adsorbed on Mg substrate. Finally, charge density distributions were realized to verify the distinguished effects of most *3d* and *4d* transition metals in terms of their catalyzer effects.

Keywords: Magnesium Hydride, Hydrogen Storage, First Principles, Molecular Dynamics, Surface Adsorption.

ÖZ

TEMEL PRENSİPLER YÖNTEMİYLE HİDROJEN DEPOLAYICI YENİ MAGNEZYUM ALAŞIMLARININ TASARIMI

Keçik, Deniz

Yüksek Lisans, Metalurji ve Malzeme Mühendisliği Bölümü

Tez Yöneticisi: Prof. Dr. M. Kadri Aydınol

Temmuz 2008, 66 sayfa

İdeal bir hidrojen depolayıcı malzemede aranılan özellikler, temel olarak yüksek depolama kapasitesi ve hızlı dehidrülendirme kinetiğidir. Bu anlamda, yavaş dehidrülendirme kinetiğine ve hidrojeni yüksek sıcaklıkta bırakmasına rağmen; magnezyum hidrür (MgH_2) ağırlık bazında % 7,66 depolama kapasitesi ile öne çıkan bir malzemedir. Dolayısıyla bu çalışmada amaç, hacim içi ve yüzey yapılarında, dehidrülendirme kinetiğinde iyileştirme sağlayan alaşım elementlerini sistematik bir biçimde incelemektir. Temel prensipler yöntemiyle yapılan hesaplamalarda, alaşımlanan magnezyum hidrür yapılarının hidrülendirme reaksiyon enerjileri hesaplanmış, saf MgH_2 'ye göre hangilerinin mutlak olarak oluşum enerjilerini düşürdüğü saptanmıştır. Buna göre, otuz iki adet element içerisinde, Sr haricindekilerin bir düşüşe sebep olduğu, bir diğer deyişle hidrür kararlılığını azaltabileceği gözlenmiştir (hidrülendirme enerjisinde yaklaşık 37 kJ/mol- H_2 'ye kadar bir düşüş olduğu saptanmıştır). Bu bağlamda öne çıkan

elementler; P, K, Tl, Si, Sn, Ag, Pb, Au, Na, Mo, Ge ve In olarak sıralanabilir. Çalışmanın diğer kısmında, çeşitli biçimlerde alaşımlandırılmış Mg ve MgH₂ yüzeylerinde, temel prensipler psödopotansiyel ve moleküler dinamik yöntemleri kullanılarak hesaplamalar yapılmıştır. Buna göre, Mo ve Ni elementlerinin, -9.2626 and -5.2995 eV olarak hesaplanan soğurulma enerjileri doğrultusunda yüzeye tutunma olalıkları yüksek olan elementler arasında oldukları görülmüştür. Buna ek olarak, yine sistematik bir biçimde, seçilen alaşım elementlerinin magnezyum yüzeyinde hidrojenin ayrışmasına ne gibi bir etki göstereceği moleküler dinamik yöntemiyle incelenmiştir. Buna göre, Co elementinin hidrojeni atomlarına ayrıştırması için 50 fs geçtiği ve hidrojen atomlarından birinin derhal yüzeye çekildiği görülmüştür. Son olarak, yüzeyde çalışılan yük dağılımı farklılıklarının 3*d* ve 4*d* geçiş elementlerinin katalizör etkisi göstermedeki başarılarını destekler nitelikte olduğu bulunmuştur.

Anahtar kelimeler: Magnezyum Hidrür, Hidrojen Depolama, Temel Prensipler, Moleküler Dinamik, Yüzey Soğurulması.

ACKNOWLEDGEMENTS

I would like to thank my supervisor, Prof.Dr. Kadri Aydınol, whom I owe greatly for every single piece of information he taught me. Thank you very much for giving me this great opportunity to get into the exciting world of atomistic modelling. I deeply appreciate your priceless guidance, support and motivation to share every bit of your knowledge and ideas until the very end.

I also wish to thank Prof.Dr. Ömer Anlağan for being a role model ahead since my childhood, with his wisdom and utterly sweet attitude. I wish to extent my thanks to Prof.Dr. Pamir Alpay for his embracing support, even from continents afar.

My utmost and sincere thanks go to my family; Abdullah, Yüksel and Defne Keçik for their extreme contribution in making me an independent and confident person by their invaluable advices and guidance, and all their unconditional love and support.

I am deeply indebted to my dearest friends Burcu Ünsal, Görkem Yılmaz, Özge Ekim, Özgecan Ulak and Sedef Çift for every sweet and sad moment we lived and shared. You are more than like sisters to me.

I would also like to express my sincere gratitude to my former lab mates, Alper Kınacı and Fatih Şen, for giving me a warm welcome, for their guidance and all the fun we had since then.

I would like to thank my friends at METE, particularly to Afshin Izanlou, Ali Erdem Eken, Elvan Tan, Emre Ergül, Ergin Büyükakıncı, Hasan Akyıldız, Metehan Erdoğan, Rabia Ölmez, Serdar Tan, Taylan Örs, Turgut Kıırma, Volkan Kalem and Volkan Kayasü (please note the alphabetical order) for their friendship and all the good times we had.

I also gratefully acknowledge my dear friends Evren Tan, Güher Kotan, Gülhan Çakmak and Barış Akgün for letting me leave METE with such warm and lovely memories.

I would like to express my deep gratitude to my dear friend Çağla Özgıt for always being there with me, providing her endless love and support and also helping me with her natural gift with the technical aspects of this dissertation.

Finally, my very special thanks go to Arda Çetin, for his continuous encouragements and sincere belief in me during the entire dissertation period. It would have been much more difficult and dull without your contribution. Thank you for the bliss and peace in my life.

I would also like to acknowledge Ulakbim High Performance Computing Center at the Turkish Scientific and Technical Research Council (TUBITAK) for providing their computing facilities for the numerical calculations performed in this study.

This work was supported by The Scientific and Technological Research Council of Turkey (TUBITAK) project no. 106M174.

TABLE OF CONTENTS

ABSTRACT.....	iv
ÖZ.....	vi
ACKNOWLEDGEMENTS.....	viii
TABLE OF CONTENTS.....	x
LIST OF TABLES.....	xii
LIST OF FIGURES.....	xiii
CHAPTERS	
1. INTRODUCTION.....	1
1.1 Hydrogen as an energy carrier.....	1
1.2 Metal hydrides.....	2
1.3 First principles methods.....	6
2. HYDROGEN STORAGE MATERIALS.....	7
3. MANY BODY PROBLEM.....	12
3.1 Density Functional Theory.....	12
3.2 Pseudopotentials:.....	16
3.2.1 PAW vs. US-PP potentials:.....	17
3.3 k -point sampling.....	17

4. AB INITIO MOLECULAR DYNAMICS	20
4.1 Born-Oppenheimer molecular dynamics	21
4.2 Car-Parrinello molecular dynamics	22
5. METHODOLOGY	23
5.1 Computational Details	24
5.1.1 Bulk magnesium hydride	24
5.1.2 Surface relaxations of magnesium (0001) and magnesium hydride (001) systems	26
5.1.3 Surface molecular dynamics on magnesium (0001) system	30
6. RESULTS & DISCUSSION	33
6.1 Bulk magnesium hydride calculations	33
6.1.1 Hydride formation energies	36
6.2 Surface calculations on magnesium and magnesium hydride systems	39
6.2.1 Molecular dynamics calculations	39
6.2.2 Ionic relaxations on surface structures	51
6.2.2.1 Substitutional adsorption on magnesium (0001) and magnesium hydride (001) surfaces	52
6.2.2.2 On-surface adsorption on Mg (0001) surface	53
6.2.2.3 Work-function calculations	55
7. SUMMARY & CONCLUSION	61
REFERENCES	63

LIST OF TABLES

TABLES

Table 1.1 Hydrogen densities of several storage materials [4].....	4
Table 5.1 Systems, related supercell sizes, number of atoms and <i>k</i> -point sampling used for ionic relaxation and MD calculations.....	32
Table 6.1 Experimental and calculated cell parameters and total energies of the alloying elements.....	34
Table 6.2 Cell parameters, total energies and formation energies of Mg hydrides.....	37
Table 6.3 Summary of the results of surface calculations, with energies in eV	59

LIST OF FIGURES

FIGURES

Figure 1.1 P-C-T and van't Hoff curves, vertical axes representing the corresponding hydrogen pressure [2].....	5
Figure 5.1 Tetragonal bulk MgH ₂ structure.....	25
Figure 5.2 Front and top views of Mg (0001) surface structure, representing substitutional adsorption.....	27
Figure 5.3 Front and top views of MgH ₂ (001) surface structure, representing substitutional adsorption.....	28
Figure 5.4 Top view of Mg (0001) surface structure, representing on-surface adsorption.....	30
Figure 5.5 Molecular dynamics cell of (0001) surface of Mg, from front and top views.....	31
Figure 6.1 Trends in hydrogen dissociation through alloying elements.....	43
Figure 6.2 The variation of separation between H atoms and z coordinates of either H atom throughout the simulation for the mentioned surface structures.....	46
Figure 6.3 Charge density difference illustrations of the selected Mg surface structures.....	49

Figure 6.4 Isosurfaces of charge density difference taken at the alloying element site for magnesium surface structures alloyed with Co and Zr elements.....	51
Figure 6.5 Sites of preference for normal adsorption on Mg (0001) surface	56
Figure 6.6 Sites of preference for adsorption on Mg (0001) surface	57
Figure 6.7 $\Delta\Phi$ values of substitutionally alloyed Mg (0001) surfaces	60

To my beloved family & dearest friends

CHAPTER 1

INTRODUCTION

1.1 Hydrogen as an energy carrier

Tremendous consumption of the fossil fuels and consequent environmental pollution in recent years, have naturally turned the attention of humankind towards alternative energy sources. Under the circumstances that oil and natural gas usage continues at this rate, fossil fuel reserves are expected to diminish by the year 2030 [1]. Furthermore, today harm given by the fossil fuel combustion products; such as carbon dioxide, nitric and nitrous oxides, sulfur dioxide and hydrocarbons is at considerably high levels. *Hydrogen* in this respect is an environmentally benign, safe and attractive medium; being the most abundant element in the universe, with a high energy density per unit weight (chemical energy of hydrogen; 142 MJ/kg is at least three times larger than that of other chemical fuels [2]) and water as the major by-product of its combustion. A method of utilizing hydrogen is to dissociate water into hydrogen and oxygen, which is an energy emitting process. Therefore, hydrogen is not considered to be the energy source itself, but is described as an *energy carrier*. In order to obtain hydrogen from raw materials (coal, water, etc.), various renewable sources of energy which could be harnessed are solar energy, wind power, hydroelectric, biomass, nuclear, geothermal, etc. [3]. Alongside the advancements within space applications, the highly efficient use of hydrogen in fuel cells to generate

electricity urged the automobile industry to invest in the progress of hydrogen energy technology. However, convenient storage of hydrogen remains a major challenge, due to the requirement of densification either into liquid or solid forms. Both liquefaction and solidification consume a significant amount of the energy contained in hydrogen, as well as the energy needed to preserve the liquid and solid states.

Today, storing hydrogen in pressurized gas and cryogenic liquid forms generally remains beyond the scope of up-to-date studies, whereas the third class of solid-state storage has received more attention lately. This final group is based upon the chemical or physical combination of hydrogen with the materials in question; which are metal/complex hydrides and carbon based structures. Of all kinds of hydrogen storing materials, metal hydrides are seen to be the promising, rather efficient and safe storage media for on-board vehicle applications. A major drawback is in the way that; they store only about 2 % to 7 % hydrogen by weight, which also brings an economic burden. Nevertheless, their volumetric storage density is higher than most of other forms of storage [4]. Brief introductory information on solid-state storage, predominantly on metal hydrides, is presented in the next section.

1.2 Metal hydrides

Metal hydrides are known to provide much safer and efficient hydrogen storage media, with respect to storing in gaseous or liquid forms. In order to achieve the optimum storing conditions, there are several attributes that a hydride material should satisfy. In this regard, Ivey and Northwood [5] have claimed the required criteria which hydride materials should attain as:

- high storage capacity
- good hydrogenation/dehydrogenation kinetics
- safety

- cycling without change in temperature and pressure during life time
- small hysteresis of P-C-T curves
- resistance to surface poisoning against pollutants
- low cost

Among various kinds of metal hydrides (including intermetallics); magnesium hydride (MgH₂) is a promising medium being light-weight, economic and having a relatively high storage capacity of 7.66 wt. %. However, due to the strong interaction in between magnesium (Mg) and hydrogen (H) (some covalent bonding character is displayed), high desorption temperatures on the order of 300 °C at 1 atm are required, which give rise to unacceptable costs of energy. Furthermore, LiAlH₄ is an example to complex hydride materials containing high H content (10.6 wt. %, also see Table (1.1)). Unfortunately, poor reversibility and slow dehydrogenation kinetics are the main drawbacks of complex hydrides. Therefore, despite their high storage capacities per weight, complex metal hydrides are different from metal hydrides in the way that they do not possess the same ease in reversibility. Table (1.1) presents some examples to the storage capacities of several materials on volumetric and gravimetric basis.

The typical metal hydride formation reaction is expressed as:



where M stands for the metal, H₂ hydrogen molecule and MH_x the metal hydride formed. x denotes the molar ratio of hydrogen to metal. Generally this reaction is seen to be exothermic, thus thermodynamically feasible and reversible in the backward direction; meaning that H₂ could be recovered upon application of heat.

Table 1.1 Hydrogen densities of several storage materials [4]

Medium	Vol. hydrogen density, 10^{22} atoms/cm ³	Gravimetric densities, wt %
H ₂ gas, 10 MPa	0.5	100
H ₂ liquid, 20 K	4.2	100
H ₂ solid, 4.2 K	5.3	100
H ₂ O liquid, RT	6.7	11.2
LiH	5.9	12.6
LiAlH ₄	5.7	10.6
MgH ₂	6.7	7.6
TiH ₂	9.2	4.0
VH ₂	11.4	3.8
Mg ₂ NiH ₄	5.9	3.6
FeTiH ₂	6.0	1.9
LaNi ₅ H ₇	7.6	1.6
PdH _{0.6}	4.3	0.6

The characteristics of metal-hydride systems could be best represented by a pressure-composition-temperature (P-C-T) diagram [5]. These diagrams are derived by keeping the temperature constant and measuring the amount of hydrogen desorbed as well as the pressure at which desorption occurs. A sample plot for LaNi₅ is given in Fig. (1.1). Initially, hydrogen goes into solid solution with the single phase named as α -phase. After the steep region of the curve, the slopy part represents the initiation of metal-hydride (or β -phase) formation, during which the pressure remains constant leading to a "plateau". This plateau continues so long as the two phases coexist, the length of which implies the amount of H₂ that could be stored by the host metal. Next, within pure β -phase, H₂ pressure is seen to be increasing together with the concentration. Temperature at which the two-phase region ends is T_c , above which α -phase is continuously converted into β -phase. The equilibrium (plateau) pressure is strongly dependent on temperature such that; when T is increased, the miscibility gap becomes narrower and higher plateau pressures are achieved. Changes in enthalpy and

entropy (ΔH and ΔS) within hydrogenation of metals are effective in the equilibrium pressure, as function of T , in a way that could be explained by the van't Hoff equation, where R is the gas constant:

$$\ln P = \frac{\Delta H}{RT} - \frac{\Delta S}{R} \quad (1.2)$$

The entropy change (ΔS) for all metal-hydrogen systems is ~ 130 J/K-mol upon hydrogen dissolution [2], where ΔH amount required to obtain 1 bar at 300 K was stated to be 19.6 kJ/mol-H [6]. Figure (1.1) displays P-C-T and van't Hoff (logarithm of plateau pressure vs. $1/T$) plots of LaNi_5 , where the hydride formation energy could be derived from the slope of van't Hoff curve.

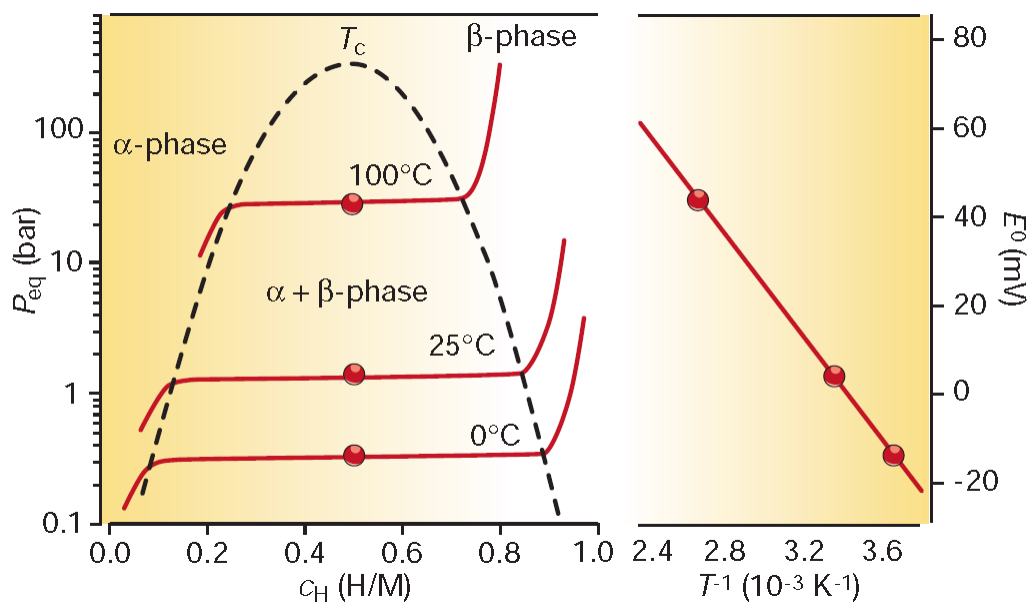


Figure 1.1 P-C-T and van't Hoff curves, vertical axes representing the corresponding hydrogen pressure [2]

Undesirable poor hydrogen desorption kinetics of some metal hydrides have tried to be remedied by several studies so far. In this respect, there are some well

known techniques which are altering the chemical composition, mechanical alloying, addition of catalysts, etc. in order to improve the hydrogenation/dehydrogenation thermodynamics. A selective literature review regarding the hydrogen storing materials, focused mostly on magnesium hydride, from both experimental and computational points of view is included in the next chapter. Prior to the presentation of this brief review, it will be useful to make an introduction to the philosophy behind *ab-initio* methods.

1.3 First principles methods

The Latin term *ab initio* means from the beginning and relies on basic and established laws of nature without additional assumptions or special models. First-principles methods have emerged in the last two decades with the evolution of computational power. This tool has been developed to serve for the calculation and prediction of several properties of condensed matter systems, via solving the Schrödinger equation numerically. The most appealing characteristic of *ab initio* methods is that no experimental data are required in order to perform a calculation. The density-functional theory (DFT) enables computations on an accurate basis, and can be combined with molecular dynamics to solve problems within dynamical and thermodynamic phenomena at metal surfaces, such as premelting and blocked melting, atomic diffusion, and catalytic reactions.

CHAPTER 2

HYDROGEN STORAGE MATERIALS

The reversible storage of hydrogen for both stationary and mobile applications could be in several forms; such as gaseous, liquid, physisorption in carbon nanotubes, metal and complex hydrides [7]. Besides the advantage of readily reacting with hydrogen, several metals, in hydride form, are capable of storing hydrogen in large amounts on a reversible basis [2]. The generally searched criteria for an ideal metal hydride are; high storage capacities, fast hydrogenation/dehydrogenation kinetics, low desorption temperatures as well as low cost. In this regard, several materials for storing hydrogen in order to achieve these criteria have been studied until today. In the followings, a selective review of literature on metal/complex hydride systems, predominantly on MgH_2 is presented.

Lithium amide system ($LiNH_2$) is known as a promising hydrogen storing medium, with a theoretical storage capacity of 11.5 wt. %, however a significantly high desorption temperature above 400 – 500 °C is observed. Jin and Wu [8] have studied the effect of doping on hydrogen desorption temperature; where they have concluded that upon substitution of Al instead of Li; the bond strength between N and H was reduced besides the observation of metal-like behavior in the system; which points out the decline in desorption temperature. Furthermore, another study related to the complex hydrides is of Dompablo and Ceder [9], which is on alanate structures; AMH_4 and A_3MH_6 ($A = Li, Na, K$ and $M = B, Al,$

Ga). It has been claimed that the stability of AMH_4 hydrides is decreased by the substitutional elements mentioned, in the order of $B > Al > H$ (coherent with the strength of covalent bonds between these and H). Also, Li substitution was found to decrease the hydrogen affinity of $NaAlH_4$ and Na_3AlH_6 systems, whereas K was seen to apply a reverse effect.

In order to decrease the hydrogen desorption temperature of MgH_2 which is above $300\text{ }^\circ\text{C}$, there are several methods such as mentioned before, like changing the chemical composition, mechanical alloying via ball-milling and addition of catalysts. Mg hydride, is known to be a promising material being economic, light weight and storing high amounts of hydrogen (7.66 wt. %) despite its high reactivity towards air and oxygen and high thermodynamical stability, which leads to poor hydriding/dehydriding kinetics [5].

There are several studies searching the ways for reducing Mg hydride stability. Song *et. al.* [10], for instance, have found out the decreasing effects of Cu, Ni, Al, Nb and Fe to Ti, in terms of descending effectiveness order, on stability of Mg hydride, via total energy methods. Furthermore, the analysis of density of states (DOS) and charge distribution results proved that the bonds between Mg and H were weakened due to the effects of alloying elements.

Vegge and his co-workers [11] deduced that; within the calculations regarding $MgTMH_3$ (TM = transition metals) hydrides with perovskite structure, the stability of alloyed hydrides tend to decrease from MgSc to MgFe, where Cu and Zn as impurity elements were not seen to make the same effect.

Alongside these studies on bulk MgH_2 , many more have been carried out on surface structures. Zaluska *et. al.* [12] pointed out the two major reasons for poor dehydrogenation kinetics; as the oxide layer formed and slow dissociation rate of hydrogen on magnesium surface. It was also mentioned that since the MgO layer impedes hydrogen penetrating inside the surface, the oxide layer needs to be

cracked by annealing at a temperature above 400 °C; so that the metal surface would be exposed to hydrogen. Furthermore in their study, the conclusion has been raised that small amounts of catalysts (like Pd or Fe) would induce the improvement of hydrogenation kinetics.

Besides palladium [12], Baer *et. al.* [13] claimed that nickel is also an outstanding catalyst since it holds the ability to dissociate and adsorb the hydrogen molecule. Titanium and vanadium, as stated by Liang *et. al.* [14], are as well favored catalysts for hydrogen absorption. Although their strong tendency towards oxidization makes the catalytic effect disappear; oxide formation is prevented once Ti and V hydrides are formed (via mechanical milling of MgH₂ by these elements). Thus, the effect of catalysis on chemisorption could still be in question.

Moreover, addition of oxide catalysts, such as Cr₂O₃, V₂O₅ and Fe₃O₄ [15], was found useful in achieving improved hydriding properties at lower temperatures. Dornheim *et. al.* [16], have stressed the effect of *3d* transition metals in their study, in terms of the reduction of hydride formation enthalpies. Nevertheless, alloying with *3d* elements gives rise to the decline in hydrogen storage capacity below 3.6 wt. %.

Sprunger and Plummer [17], on the other hand, executed a study based on the comparison of experimental and theoretical results. Regarding the interaction of H₂ with Mg (0001) surface, the tools benefited were electron energy loss spectroscopy (EELS), thermal desorption spectrometry (TDS), core spectroscopy and work-function measurements. In their study, as a result of the exposure of pure Mg (0001) surface (≥ 110 K) to hydrogen at room temperature, not only it was unlikely to observe molecular adsorption of H₂; but also dissociative chemisorption did not take place under the temperature conditions in question. High activation barrier for H/simple metal systems derived from the theoretical calculations are stated to be in coherence with this result.

Bird *et. al.* [18] indicated that; as a result of the interaction between hydrogen and metal surface, the non-bonding orbital of the metal is being filled. Moreover, their study revealed that with a barrier of 0.4 eV, the adsorption site preferred by H₂ is the bridge site between the two metal atoms. Furthermore, Ravindran *et. al.* [19] have studied complex hydrides, making use of charge density, charge transfer, electron localization function, partial densities of states, Mulliken population analysis, and Born effective charges. Finally, they have reached the conclusion that; due to their weaker bonding characteristics, the interstitial sites are favored by hydrogen in metals, alloys and intermetallic structures.

In another study of Vegge [20], where he made use of the nudged elastic band method (NEB), he presented the rate-limiting step for absorption of hydrogen on Mg (0001) surface as the dissociation, whereas that for desorption was concluded to be the rejoining of H₂. The potential energy surface (PES) results for hydrogen action on magnesium put forward the rate-limiting character of dissociation step by yielding large activation energies for this and diffusion of dissociated hydrogen into the first layer of Mg slab.

Pozzo *et. al.* [21] examined the interaction of Ni and Ti elements and H₂ molecule at the (0001) surface of Mg and configured the efficiency of both in terms reducing the activation barrier for hydrogen dissociation. Moreover, they have concluded that Ni is both accomplished on catalyzing the dissociation and diffusion of hydrogen over Mg surface; whereas Ti only acts in enhancing the dissociation characteristics of H₂.

Apart from the studies on hydrogen interaction with magnesium surface, Kiejna *et. al.* [22], have examined the adsorption of low-coverage alkali adatoms on (0001) surface of Mg. The results display that; potassium would prefer hollow sites, where its relatively large size disables the adsorption on substitutional sites.

In this study, we aimed to investigate the manners for destabilizing of MgH_2 as well as the hydrogen dissociation and adsorption on Mg surface and suggest a systematic within the periodic table in terms of the catalyzer effects of selected elements. Correspondingly, hydride formation energies of alloyed Mg hydride structures, substitutional and on-surface adsorption energies regarding Mg (0001) surfaces doped with one adatom, were computed via the ab initio total energy pseudopotential methods. In addition, first principles molecular dynamics calculations were performed for surface structures also including the hydrogen molecule. Also, charge density difference distributions were illustrated for substitutionally alloyed Mg surface systems, and work-function values on substituted Mg surfaces were calculated.

CHAPTER 3

MANY BODY PROBLEM

3.1 Density Functional Theory

The fundamental tenet of density functional theory (DFT) is that any property of a system of many interacting particles can be viewed as a functional of the ground state density $n_0(\mathbf{r})$; that is one scalar function of position $n_0(\mathbf{r})$, in principle, determines all the information in the many-body wavefunctions for the ground state and all excited states. The original formulation of density-functional theory for application to quantum systems is embodied in two fundamental pieces of work: the *Hohenberg-Kohn theorems* [23] and the *Kohn-Sham mapping* [24]. Since these techniques have become popular in applications, a number of comprehensive reviews of DFT and its implementations exist in the literature (e.g. [25,26]). The Hohenberg-Kohn theorems, published in 1964, together with the Kohn-Sham mapping, published in 1965, provide a computationally convenient reformulation of the quantum mechanical problem of a system of N interacting electrons. The first Hohenberg-Kohn theorem legitimizes the use of the electronic density $n(\mathbf{r})$ as a fundamental quantity to specify the state of a system, by showing that there is a one-to-one correspondence between the charge density of the system of electrons and the external potential $v(\mathbf{r})$ acting on that system. The second Hohenberg-Kohn theorem demonstrates that the ground state energy of an electronic system is determined by a functional $E[n(\mathbf{r})]$ of the

electronic density; for a given external potential, this functional is a minimum for the ground state density $n_0(\mathbf{r})$, and it gives the ground state energy of the system E_0 . Denoting the external potential by $v_{\text{ext}}(\mathbf{r})$, the interaction of the electronic charge density with the external potential can be separated out in the total energy functional:

$$E[n(\mathbf{r})] = F[n(\mathbf{r})] + \int \vartheta_{\text{ext}}(\mathbf{r}) n(\mathbf{r}) \, \text{d}\mathbf{r} \quad (3.1)$$

$F[n]$ is the density functional of DFT, and it can be shown that it does not depend explicitly on the external potential - hence it is a *universal* functional of the charge density. The Hohenberg-Kohn theorems allow us in principle to move away from a description based on the N -body wavefunction (dependent on $3N$ variables) to a description based on the density $n(\mathbf{r})$ alone, a function of only three variables. In practice, even though the density functional $F[n]$ is perfectly well defined, its explicit dependence on the charge density is not known. Approximations to $F[n]$ have been found to correctly describe several systems, such as *sp*-bonded metals. Recent applications are included in references [27-29]. The Kohn-Sham approach allows us to recover an accurate description of the main contributions to the total electronic energy (i.e. the quantum kinetic energy and the electrostatic Hartree contributions), with the help of a mapping of the true system of N *interacting* electrons onto a fictitious system of N *non-interacting* electrons, with the density $n(\mathbf{r})$ of the fictitious system being equal to that of the real one. A set of N orthonormal single-particle orbitals $\{\psi_i\}$ (the Kohn-Sham eigenstates) is thus introduced, such that the density (of both systems) is given by:

$$n(\mathbf{r}) = \sum_{i=1}^N \varphi_i^*(\mathbf{r}) \varphi_i(\mathbf{r}) \quad (3.2)$$

The universal functional $F[n(\mathbf{r})]$ is then decomposed as follows:

$$E[n] = T_s[n] + E_H[n] + \int \vartheta_{\text{ext}}(\mathbf{r}) n(\mathbf{r}) \, \text{d}\mathbf{r} + E_{xc}[n] \quad (3.3)$$

in which:

$$T_s[n] = -\frac{1}{2} \sum_{i=1}^N \int \varphi_i^*(\mathbf{r}) \nabla^2 \varphi_i(\mathbf{r}) \, d\mathbf{r} \quad (3.4)$$

is the kinetic energy of the non-interacting electronic system; the Hartree term:

$$E_H[n] = \frac{1}{2} \int d\mathbf{r} \int d\mathbf{r}' \frac{n(\mathbf{r}) n(\mathbf{r}')}{|\mathbf{r}-\mathbf{r}'|} \quad (3.5)$$

takes account of the Coulomb interaction of the charge density, and the external potential $v_{ext}(\mathbf{r})$ is that due to the nuclei:

$$\vartheta_{ext}(\mathbf{r}) = -\sum_i \frac{Z_i}{|\mathbf{R}_i-\mathbf{r}|} + \sum_{i<j} \frac{Z_i Z_j}{|\mathbf{R}_i-\mathbf{R}_j|} \quad (3.6)$$

The final term E_{xc} in Eq. (3.3) is the *exchange-correlation* energy, operationally defined as the difference between the first three terms on the right-hand side of the equation and the exact energy of the system. The form of this universal exchange-correlation functional is unknown, and it contains most of the many-body complexity of the interacting electron gas. Still, its value in absolute terms is comparatively small, and, most importantly, simple approximations to it have proved to be reasonably accurate for a great variety of applications. According to the second Hohenberg-Kohn theorem, the energy functional $E[n]$ in Eq. (3.3) must be minimized with respect to the density $n(\mathbf{r})$ (subject to the constraint of charge conservation) to find the ground state density and total energy. The minimum condition can be written as:

$$\delta[T_s[n] + E_H[n] + \int \vartheta_{ext}(\mathbf{r}) n(\mathbf{r}) \, d\mathbf{r} + E_{xc}[n] - \mu(\int n(\mathbf{r}) \, d\mathbf{r} - N)] = 0 \quad (3.7)$$

where the Lagrange multiplier μ has been introduced to take account of charge conservation and orthonormality of the orbitals. Defining the Kohn-Sham effective potential $v_{KS}(\mathbf{r})$,

$$\vartheta_{KS}(\mathbf{r}) = \vartheta_{ext}(\mathbf{r}) + \int \frac{n(\mathbf{r}')}{|\mathbf{r}-\mathbf{r}'|} \, d\mathbf{r}' + \vartheta_{xc}(\mathbf{r}) \quad (3.8)$$

in which

$$\vartheta_{xc}(\mathbf{r}) = \frac{\delta E_{xc}[n(\mathbf{r})]}{\delta n(\mathbf{r})} \quad (3.9)$$

Finally, evaluating the functional derivative, the Euler-Lagrange equations for the constrained minimization problem, known as the *Kohn-Sham equations*, are obtained:

$$\left[-\frac{1}{2}\nabla^2 + \vartheta_{KS}(\mathbf{r}) \right] \varphi_i(\mathbf{r}) = \epsilon_i \varphi_i(\mathbf{r}) \quad (3.10)$$

A common approach to solving the Kohn-Sham equations is by iterative evolution of some reasonable trial set of orbitals. Alternatively, the minimization problem they represent (that is finding the minimum of the total energy functional) can be solved by direct methods, such as the conjugate gradient technique [25]. As noted above, the form of the exchange-correlation functional in Eq. (3.3) is unknown, so an approximation is needed. A number of such approximations for the exchange - correlation energy functional have been published; well-known and reliable ones are the *local density approximation* (LDA), that was in fact originally suggested in the paper of Kohn and Sham [30], and the *generalized gradient approximation* (GGA) [31]. The local density approximation considers the exchange-correlation energy in each volume element $d\mathbf{r}$ at \mathbf{r} (where the density is $n(\mathbf{r})$) to be that of a homogeneous electron gas of density n :

$$E_{xc}^{LDA}[n(\mathbf{r})] = \int \epsilon_{xc}(n) n(\mathbf{r}) d\mathbf{r} \quad (3.11)$$

where $\epsilon_{xc}(n)$ is the exchange-correlation energy per unit density of a homogeneous electron gas at constant density n . As their name suggests, the generalized gradient approximations include terms dependent on gradients of the charge density in the expression for the exchange-correlation functional. The Hohenberg-Kohn-Sham density-functional theory formalism described above has become very popular for implementation in computational codes and a great number of practical applications have been made using it.

The method avoids the problem of determination of the ground-state wave function and the central role is played by the electronic density $n(\mathbf{r})$. The electron density in a metal is connected with the one-electron wave functions \mathbf{r} by the following sum over the occupied states.

3.2 Pseudopotentials:

The widespread use and success of DFT in predicting materials properties during the last decade stems largely from the successful application of pseudopotentials (PPs). Replacing explicit treatment of the chemically inert core electrons with an effective core potential, i.e. a PP, reduces the variational degrees of freedom and avoids the numerical challenge of rapid spatial variations in the electronic structure. Hence, efficient numerical techniques, particularly fast Fourier transform methods underlying plane wave basis codes, can be used. The theory of PPs is well-founded, but the practice of constructing transferable and efficient PPs is less developed. Methods for generating PPs include the generalized norm conserving pseudopotentials (GNCPPs) of Hamann [32], softer PPs by Troullier-Martins (TM) [33] and Vanderbilt's non-norm-conserving ultra-soft PPs (USPPs) [34]. Even minor variations of a parameter can have major effects on computed properties and, as we shall demonstrate, a PP that may appear to be perfectly adequate in one chemical environment can fail badly in another. The appropriate figure of merit for the quality of a PP is not how well it matches experiment, but how well it reproduces the results of otherwise identical AE calculations. In principle, the results of a DFT calculation should not be affected by using PPs instead of AE potentials. In practice, of course, this replacement is never perfect. Issues inherent to standard NCPPs are broadly relevant to all PPs. Design of workable non-norm-conserving ultra-soft potentials, or their close relatives, projector augmented-wave (PAW) potentials [35], presents additional challenges.

3.2.1 PAW vs. US-PP potentials:

In the following, a brief comparison of the characteristics of PAW and US-PP potentials is given:

- PAW potentials are generally of similar hardness across the periodic table.
- Most of the PAW potentials were optimized to work at a cutoff of 250-300 eV.
- PAW potentials are usually slightly harder than US-PP.
- For US-PP the core radii were chosen according to the covalent radius (periodic table)
- US-PP becomes progressively softer when one moves down the periodic table.
- For one-component systems, US-PP is slightly faster (at the price of a somewhat reduced precision)
- For compounds, where species with very different covalent radii are mixed, the PAW potentials seem to be superior.

3.3 k -point sampling

First-principles total energy calculations require integrals of wavefunctions and/or eigenvalues over the Brillouin zone. Thus, the total energy of a crystal is given by:

$$E = \sum_{n \in \text{occ.}} \int_{\text{B.Z.}} \varepsilon_n(\mathbf{k}) d^3k \quad (3.12)$$

where the sum is over the occupied states of the system at the wave vector k in the first Brillouin zone. In practice the integral must be approximated by a sum over selected k -points in the Brillouin zone:

$$E \approx \sum_{i=1}^N \sum_{n \in occ.} w_i \varepsilon_n(\mathbf{k}_i) \quad (3.13)$$

where the (lattice dependent) weights w_i and points \mathbf{k}_i are chosen to reproduce the integral as accurately as possible. Common meshes are the so-called regular k -point meshes, where the points are equally spaced from the origin, and the special k -point mesh of Monkhorst and Pack, which offsets the regular mesh from the origin to reduce the number of k -points needed. In a wide variety of lattices, the original special k -point method must be modified to properly account for the symmetry of the lattice.

Electronic states are allowed only at a set of k -points determined by the boundary conditions that apply to the bulk solid. The density of allowed k -points is proportional to the volume of the solid. The infinite number of electrons in the solid is accounted for by an infinite number of k -points, and only a finite number of electronic states are occupied at each k -point. The Bloch theorem changes the problem of calculating an infinite number of electronic wave functions to one of calculating a finite number of electronic wave functions at an infinite number of k -points. The occupied states at each k -point contribute to the electronic potential in the bulk solid so that, in principle, an infinite number of calculations are needed to compute this potential. However, the electronic wave functions at k -points that are very close together will be almost identical; hence it is possible to represent the electronic wave functions over a region of k -space by the wave functions at a single k -point. In this case the electronic states at only a finite number of k -points are required to calculate the electronic potential and hence determine the total energy of the solid. Methods have been devised for obtaining very accurate approximations to the electronic potential and the contribution to the total energy from a filled electronic band by calculating the electronic states at special sets of k -points in the Brillouin zone [36-39]. Using these methods, one can obtain an accurate approximation for the electronic potential and the total energy of an insulator or a semiconductor by calculating the electronic states at a very small number of k -points. The electronic potential and total energy are more

difficult to calculate if the system is metallic because a dense set of k -points is required to define the Fermi surface precisely. The magnitude of any error in the total energy due to inadequacy of the k -point sampling can always be reduced by using a denser set of k -points. The computed total energy will converge as the density of k -points increases, and the error due to the k -point sampling then approaches zero. In principle, a converged electronic potential and total energy can always be obtained provided that the computational time is available to calculate the electronic wave functions at a sufficiently dense set of k -points.

CHAPTER 4

AB INITIO MOLECULAR DYNAMICS

In a molecular dynamics (MD) simulation, the microscopic trajectory of each individual particle in the system is determined by the integration of Newton's equations of motion. In classical MD, the system is considered to be composed of massive, pointlike particles, with forces acting between them derived from empirical effective potentials. Most forms of *ab initio* MD make a similar assumption, considering the atomic nuclei as classical particles evolving according to the Newtonian equations of motion. However, the forces acting on the nuclei are deemed quantum mechanical in nature, and are derived from accurate electronic structure calculations. Since atomic nuclei are five orders of magnitude smaller than the atoms themselves, and each nucleon is two thousand times heavier than an electron, such a classical approximation (essentially a Born-Oppenheimer decomposition of the full wavefunction into an electronic wavefunction in the presence of an external electrostatic potential due to the nuclei) is often perfectly appropriate. At very low temperatures, quantum delocalization effects can gain relevance; this can be significant for the lightest elements, such as hydrogen. More importantly, the use of classical equations of motion implies that the vibrational degrees of freedom are not quantized, and follow classical Boltzmann statistics. Such an approximation can be relevant, since at room temperature every normal mode with frequency higher than ~ 300 cm^{-1} will be affected - while in reality high-frequency modes are often effectively in their zero-point motion ground state, in a classical MD simulation they

exchange energy back and forth with all other degrees of freedom. While path - integral techniques can be used to fully describe these quantum degrees of freedom, the vast majority of applications of quantum mechanical molecular dynamics techniques consider a classical evolution of the nuclei, adiabatically separated from the electrons, with a parametric evolution for the electronic wavefunction always in the ground state with respect to the instantaneous nuclear coordinates. First-principles molecular dynamics was first introduced by Car and Parrinello [40] in 1985; its essential features will be briefly described in Section 4.2.

The Car-Parrinello approach introduces an extended Lagrangian formula to provide a simultaneous evolution of the physical (nuclear coordinates) and computational degrees of freedom (expansion coefficients for the electronic wavefunctions). Often an alternative approach is used (Born-Oppenheimer molecular dynamics), where the electronic degrees of freedom are self consistently optimized at every ionic time step, trading computational efficiency and a coherent dynamical scheme for a simpler and more resilient algorithmic implementation.

4.1 Born-Oppenheimer molecular dynamics

As mentioned before, in Born-Oppenheimer molecular dynamics (BOMD) simulations [41] use is made of the fact that the nuclei have masses significantly greater than the electrons. This mass difference means that typical nuclear frequencies are much smaller than electronic ones, so a separation between the nuclear and electronic motion is possible. Adiabaticity is assumed, whereby the electronic system relaxes instantaneously to the ground state for each configuration of the nuclei. BOMD scheme thus straightforwardly solves the static electronic structure problem for fixed nuclei at each MD step, and evolves the nuclei according to the classical Newtonian equations of motion.

4.2 Car-Parrinello molecular dynamics

The Car-Parrinello MD scheme [40] reformulates the problem of the coupled electronic and nuclear systems, beginning with an extended Lagrangian in which the electronic degrees of freedom are included as classical dynamical variables with fictitious masses.

If the fictitious masses (μ_i) for the electronic degrees of freedom are chosen to be much smaller than the nuclear masses, then a metastable separation between the evolution of the electronic orbitals and the (much slower) dynamics of the massive nuclei ensues, assuring that the nuclei act only adiabatically as a driving force for the electronic wavefunctions. Oscillations of the orbitals that are coherent with the instantaneous motion of the nuclei are favored, and the orbitals will evolve remaining close to the ground state. In practical terms, there will always be a trade-off between the choice of smaller electronic orbital masses (which will give a more responsive dynamics and preserve a quasi-adiabatic behavior but also require a small MD time step) and the requirement of keeping the time step for the integration of the equations of motion as large as possible, in order to decrease the computational cost to evolve the system for a given time. The gap in the single-particle energy spectrum determines the largest time step that will maintain the (metastable) adiabatic separation between the electronic and nuclear subsystems during the simulation. In metals there is no gap in the energy spectrum, leading to a severe breakdown of such separation. Several solutions to this problem have been proposed, from the coupling of thermostats to the electronic subsystem, to the use of mixed Car-Parrinello/ensemble-DFT approaches, to resorting to Born-Oppenheimer molecular dynamics or Born-Oppenheimer/ensemble DFT [42-46].

CHAPTER 5

METHODOLOGY

In this study, bulk and surface characteristics of magnesium in both elemental and hydride forms have been systematically investigated via the first principles pseudopotential total energy and molecular dynamics methods. The code used for this purpose is VASP (Vienna ab-initio simulation package), developed at the Institut für Materialphysik of the Universität Wien [47-49]. A plane-wave pseudopotential method based on a self-consistent density functional theory is implemented in this ab initio total energy program.

The approximation benefited in order to describe exchange-correlation energy as a functional of the density is the generalized gradient approximation (GGA), proposed by Perdew et al. [50], where the core electrons were replaced by Vanderbilt ultrasoft pseudopotentials (US-PP) [34]. The superiority of GGA (over LDA) has been reviewed in several examples, by Ziesche *et al.* [51] such that; atomization energies of molecules [52], binding energies of rare-gas dimers [53-55], lattice constants of alkali metals [56] and transition metals [57] are calculated via GGA more accurately and realistically.

5.1 Computational Details

5.1.1 Bulk magnesium hydride

For the calculations performed on bulk magnesium hydride structures, a 2x2x2 supercell composed of 16 magnesium (Mg) and 32 hydrogen (H) atoms was constructed. The supercell size which is eight times larger than a single magnesium hydride unit cell, was decided to be sufficient to attain accurate enough results in terms of the calculated energy of the system and equilibrium lattice parameters. With the aim of investigating the effects of alloying elements on several properties of bulk MgH₂ system, hydrides alloyed with thirty two different alloying elements (M) were created. While choosing the elements to be substituted inside the bulk structure, one of the criteria was to prefer the elements that are soluble in Mg at least to some extent. Therefore, binary phase diagrams of Mg-M systems were examined one by one. However, the only criterion for element choice was not only the amount of its solubility in magnesium, as many elements that have no or very little solubility were also preferred during alloying studies. As a matter of fact, alloying elements that represent characteristics of each group or row within the periodic table were tried to be selected. To be more specific, we have selected dopants from the entire 3d transition metals row, 4d transition metals row from Zr to Mo and Pd to In, some heavy metals such as Au and Pb, some alkaline elements and also some nonmetals like P and Ge.

The alloying element was substituted instead of one Mg atom at the center of each structure, resulting a concentration of 6.25 at. % M. Fig. (5.1), produced by the electronic structure drawing tool VESTA [58], exhibits the bulk magnesium hydride, with tetragonal rutile-like (TiO₂) crystal structure, where green circles denote Mg atoms and smaller pink circles stand for H atoms. Besides, the red circle at the center denotes the alloying element.

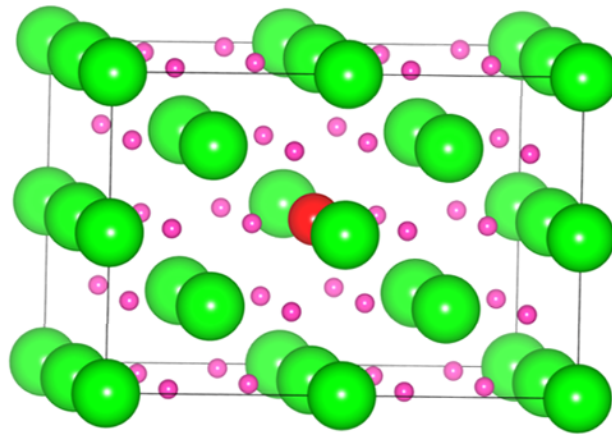


Figure 5.1 Tetragonal bulk MgH₂ structure

k-point sampling was implemented on a 6x6x6 gamma grid, which led to totally 52 irreducible *k*-points in the structure. On the other hand, unit cell calculations of each alloying element were performed on a 28x28x28 gamma grid. Even though several different settings for *k*-point sampling have been tried, finally it was deduced that as larger grids are used, the percent errors (relative to the initial, experimental values set) in the calculated lattice parameters are diminished.

Afterwards, supercell hydride and elemental unit cell systems were allowed to fully relax in terms of all atomic degrees of freedom for the purpose of obtaining the lowest energy configurations; so that the states which hydride systems are most stable were achieved. Additionally, spin polarized calculations were performed for Fe, Ni and Co doped systems where no significant effect was seen to be created energetically, with respect to the non-spin polarized calculations. After complete relaxation of the systems, total energies were recalculated for the optimized structures.

Since the main aim is to depict which elements are most effective in decreasing the magnesium hydride formation energy, hydriding energies are calculated for each of the thirty two systems. Alloyed magnesium hydride formation reaction is as follows:



Formation energies of these structures therefore are calculated via the following equation:

$$\Delta E_{bulk(hyd)} = E_{Mg_{15}MH_{32}} - (15E_{Mg} + 16E_{H_2} + E_M) \quad (5.2)$$

where E_x represent the calculated total energies of the hydride, Mg, H_2 and M respectively. Since the entropy term is ignored within the calculations carried out at the ground state (0 K), enthalpies of hydride formation reactions are approximated to the formation energies of hydrides.

5.1.2 Surface relaxations of magnesium (0001) and magnesium hydride (001) systems

Besides the studies regarding bulk magnesium hydride system, we investigated the adsorption behavior of previously mentioned alloying elements on Mg and MgH_2 surfaces. Accordingly, the calculations were performed for surface structures with a slab size of $3 \times 3 \times 3$ (thus 6 atomic layers of Mg for magnesium and 6 atomic layers composed of Mg and H for magnesium hydride structure). After trial of several vacuum distances, a vacuum range of approximately 11.5 Å was created at the top of Mg and MgH_2 surfaces, which was decided to be adequate to model the surface accurately and cover the sufficient separation between periodic images. Moreover, k -point sampling was performed on the gamma point only. Surface systems were allowed to relax in terms of all atomic degrees of freedom, with the aim of obtaining the lowest energy configurations. Here again, additional spin polarized calculations for Fe, Ni and Co doped

systems were executed and no significant effect was observed energetically, with respect to the non-spin polarized calculations.

Alloying on the surface structures in question has been implemented in two different ways. First one is the *substitutional adsorption*, in which the dopant (selected impurity elements) is inserted in place of a Mg atom at the center of the uppermost layers of Mg and MgH₂ substrates.

In the case of hexagonal Mg (0001) surface, there are 53 Mg atoms and 1 substitutionally doped M atom (creating a concentration of 0.926 at. %), as could be seen in Fig. (5.2). In the figure, blue circles represent Mg atoms where smaller one at the center of the upper-most layer is the adatom.

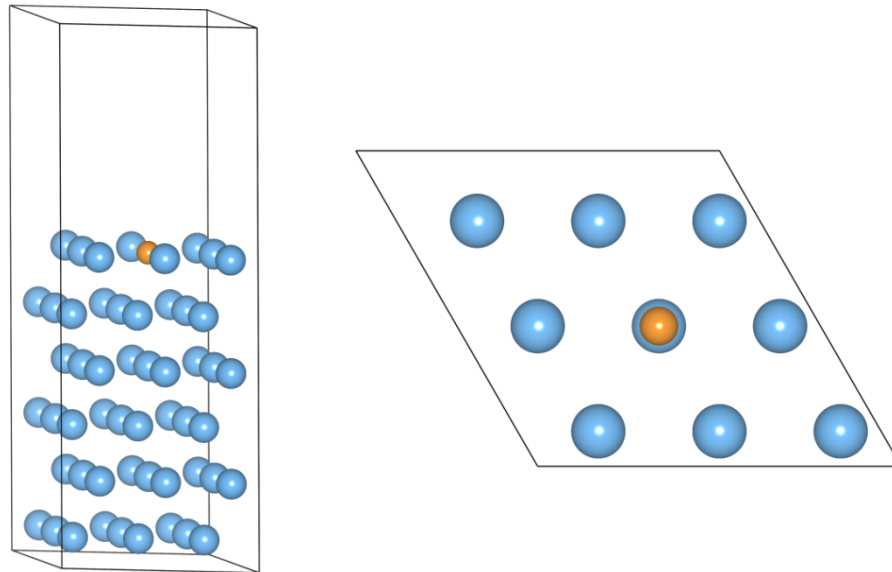


Figure 5.2 Front and top views of Mg (0001) surface structure, representing substitutional adsorption

The substitutional adsorption energy (represented by $E_{\text{sub-ads,Mg(0001)}}$) calculation for (0001) surface of Mg is via the following equation:

$$E_{sub-ads,Mg(0001)} = E_{M/Mg(0001)} - E_{Mg(0001)} - E_{M-atom} + E_{Mg-vacuum} \quad (5.3)$$

where $E_{M/Mg(0001)}$ and $E_{Mg(0001)}$ express the total energies of substitutionally alloyed and pure magnesium surface structures, respectively. E_{M-atom} represents the calculated free energy of the adatom. Besides, as also presented in the study of Neugebauer and Scheffler [59], $E_{Mg-vacuum}$ stands for the energy of Mg atom (to be substituted by M atom) which is considered to be removed from the top plane and brought to a kink site at the surface. For the calculation of this term; one magnesium atom was put on the surface at a regular lattice point of the unit cell. Next, the difference between total energies calculated for this configuration and normal Mg surface was taken; which yields the term $E_{Mg-vacuum}$.

Furthermore, there are 53 Mg, 1 M and 108 H atoms within the MgH_2 (001) surface structure constructed for substitutional adsorption of the selected adsorbates. Fig. (5.3) displays this structure clearly, where green circles denote Mg atoms and smaller pink circles stand for H atoms. Here again, the red circle at the center denotes the alloying element.

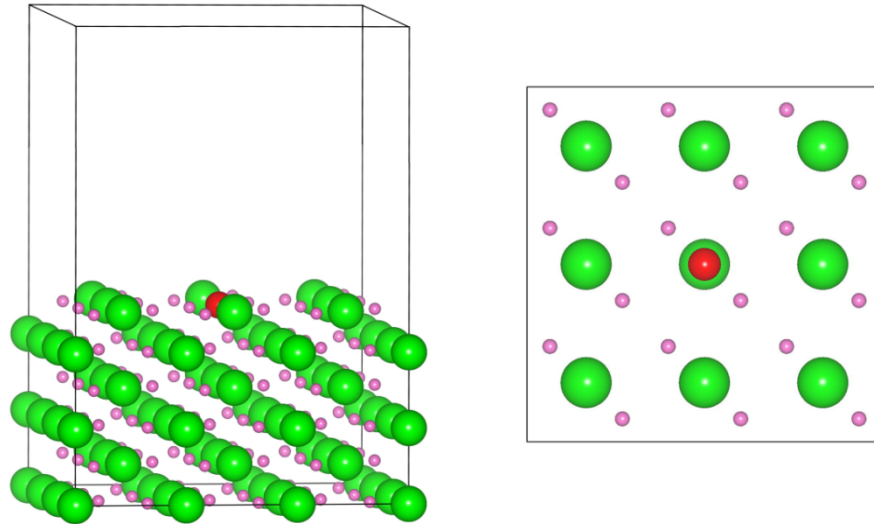


Figure 5.3 Front and top views of MgH_2 (001) surface structure, representing substitutional adsorption

The substitutional adsorption energy (expressed as $E_{\text{sub-ads,MgH}_2(001)}$) calculation for (001) surface of MgH₂ is via the following equation [59]:

$$E_{\text{sub-ads,MgH}_2(001)} = E_{M/\text{MgH}_2} - E_{\text{MgH}_2(001)} - E_{M\text{-atom}} + E_{\text{Mg-vacuum}} \quad (5.4)$$

where $E_{M/\text{MgH}_2(001)}$ and $E_{\text{MgH}_2(001)}$ represent the total energies of substitutionally alloyed and pure magnesium hydride surface structures, respectively. $E_{M\text{-atom}}$ denotes the free energy of the adatom. Moreover, $E_{\text{Mg-vacuum}}$ is for the energy of Mg atom (to be substituted by M atom) which is considered to be removed from the top plane and brought to a kink site at the surface. Here again, one magnesium atom was inserted on the surface at a regular lattice point of the unit cell. Then, the difference between total energies calculated for this configuration and normal MgH₂ surface was taken; which gives the term $E_{\text{Mg-vacuum}}$.

Furthermore, the second form of adsorption of the selected dopants, which was studied only on Mg (0001) surface, is the *on-surface* or *normal adsorption*. In this case, the alloying element is placed inside the vacuum region, slightly above (1.6 – 1.8 Å) the surface, hence not instead of a Mg atom. These systems were then relaxed, in three different positions; which are *hollow* (H), *top* (T) and *bridge* (B), as illustrated in Fig. (5.4). In this figure, large blue circles denote magnesium atoms and small circles stand for the adatoms, where positions they are placed are represented with initials.

Calculation of on-surface adsorption energies for normally doped Mg (0001) surface (expressed as $E_{\text{nor-ads,Mg}(0001)}$) is via the equation shown as follows:

$$E_{\text{nor-ads,Mg}(0001)} = E_{M/\text{Mg}(0001)} - E_{\text{Mg}(0001)} - E_{M\text{-atom}} \quad (5.5)$$

where $E_{M/\text{Mg}(0001)}$ and $E_{\text{Mg}(0001)}$ represent the total energies of normally doped and pure Mg surface structures, respectively. Here again, $E_{M\text{-atom}}$ is the free energy of the adsorbed species.

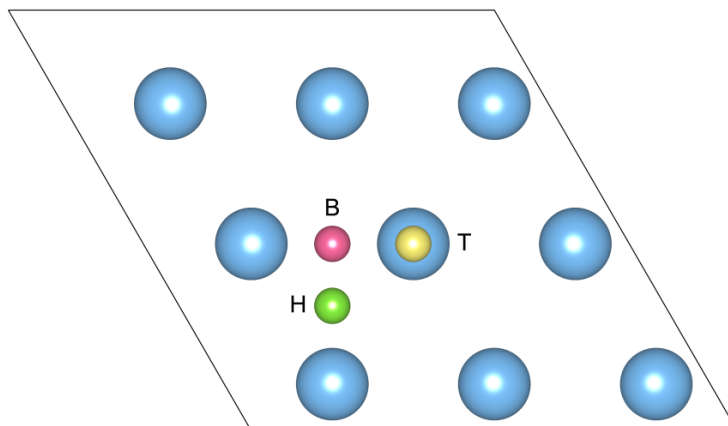


Figure 5.4 Top view of Mg (0001) surface structure, representing on-surface adsorption

5.1.3 Surface molecular dynamics on magnesium (0001) system

In the proceeding part of the study, we performed first principles molecular dynamics (MD) calculations with the motivation of determining a systematic within the hydrogen adsorption characteristics on Mg (0001) surface. Accordingly, several benchmark studies were executed prior to the achievement of optimum parameters to be set for dynamic calculations. Some examples are; doing the calculations under 573 K, applying velocity scaling only up to a number of ionic steps, varying the time-step for ion motion in between 0.2 and 1.0 fs (1 femtosecond = 10^{-15} second), enhancing or reducing the degree of precision and altering the number of ionic steps. In order to acquire as accurate and realistic results as possible, several variables/parameters could be changed such as k -points, precision, slab thickness, vacuum size, supercell (or box) size, energy cutoff value etc. However, all of these bring costs of *longer experiment time* and *higher requirement of computer capacities*, which are important criteria most of the time. Therefore, parameters that help providing closest results to the real world were tried to be selected.

For the MD calculations, a box (where the atomic positions are initially set as were found in the relaxed bulk structure of Mg) with a slab size of $3 \times 3 \times 3$, with 53 Mg atoms and 1 M atom and a vacuum range of approximately 11 \AA at the top was created. k -point implementation was performed on the gamma point only. Moreover, surface temperature controlled by a Nosé thermostat [60,61] and time-step per each ionic motion were specified as 300 K and 0.2 fs, respectively. Even though 1.0, 1.5 and 2.0 \AA as distances of H_2 molecule to the surface were set and calculations over a number of alloyed Mg (0001) systems were performed, eventually we decided hydrogen molecule to be located 1.5 \AA away from the surface, near the top of an atomic position which is occupied by an alloying element, as displayed in Fig. (5.5). In the top view, light colored large circles represent the upper-most Mg atoms at the surface (smaller is the adatom), while the sub-layer Mg atoms are indicated by dark color. Finally, upper five layers of Mg atoms were allowed to relax while the very bottom layer was kept fixed.

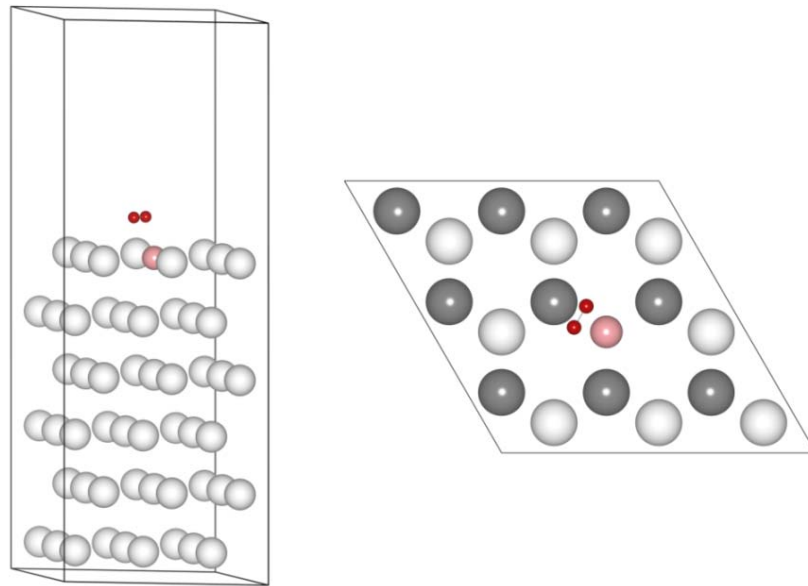


Figure 5.5 Molecular dynamics cell of (0001) surface of Mg, from front and top views

In the following, Table (5.1) introduces a brief summary of the parameters and settings used for all types of calculation in this study:

Table 5.1 Systems, related supercell sizes, number of atoms and k -point sampling used for ionic relaxation and MD calculations

System	Type of Calcul.	Supercell Size	No. Of Atoms	k -points
MgH ₂ , Bulk	Ionic Relax.	2 × 2 × 2	48 (15 Mg, 1 M, 16 H)	6 × 6 × 6
MgH ₂ , Surface	Ionic Relax.	3 × 3 × 3	162 (53 Mg, 1 M, 108 H)	1 × 1 × 1
Mg (0001), Surface	Ionic Relax.	3 × 3 × 3	54 (53 Mg, 1 M)	1 × 1 × 1
Mg (0001), Surface	MD	3 × 3 × 3	56 (53 Mg, 1 M, H ₂ in vacuum)	1 × 1 × 1

CHAPTER 6

RESULTS & DISCUSSION

6.1 Bulk magnesium hydride calculations

For the first major part of this study, thermodynamically less stable forms of MgH_2 were tried to be detected, with the aim of achieving improved hydrogen desorption characteristics. As seen from Eq. (5.1), modification in magnesium hydride structure takes place via alloying MgH_2 by the selected impurity elements (M). Calculation of the related hydride formation energies is given in Eq. (5.2). Accordingly, total energies of the alloyed hydride systems, magnesium, hydrogen molecule and impurity elements were needed to be calculated first.

Furthermore, new structural parameters for the relaxed systems with optimized geometries and energies were defined. Then, they were compared to the initially set experimental values, in order to test the success of the ab initio simulation program VASP in terms of the accuracy in prediction. In this respect, results related to the theoretically calculated and experimental cell parameters of the elements, as well as the calculated total energies of the elemental unit cell systems are given in Table (6.1).

Table 6.1 Experimental and calculated cell parameters and total energies of the alloying elements

System	Experimental values	Theoretical values	
	Cell parameters (Å)	Cell parameters (Å)	Total energies (eV/unit cell)
Mg	a = 3.213 c = 5.213	a = 3.190 c = 5.192	-3.0157
Ag	a = 4.086	a = 4.128	-10.8633
Al	a = 4.050	a = 4.036	-14.7011
Au	a = 4.072	a = 4.143	-12.7415
Ca	a = 5.559	a = 5.497	-7.7219
Cd	a = 2.979 c = 5.617	a = 3.001 c = 5.613	-1.5348
Co	a = 2.506 c = 4.069	a = 2.493 c = 4.041	-14.0924
Cr	a = 2.884	a = 2.845	-18.8625
Cu	a = 3.608	a = 3.617	-15.0218
Fe	a = 2.932	a = 2.855	-16.6017
Ge	a = 5.651	a = 5.748	-36.0809
Hf	a = 3.230 c = 5.120	a = 3.173 c = 5.017	-19.7687
In	a = 3.246 c = 4.943	a = 3.300 c = 5.027	-5.1490
K	a = 5.328	a = 5.269	-2.0591
Li	a = 3.111 c = 5.093	a = 3.033 c = 4.957	-3.8127
Mn	a = 8.894	a = 8.568	-517.9909
Mo	a = 3.145	a = 3.148	-21.6504
Na	a = 3.767 c = 6.154	a = 3.742 c = 6.106	-2.5976
Nb	a = 3.300	a = 3.288	-20.3420
Ni	a = 3.524	a = 3.514	-21.8874
P	a = 3.310 b = 10.500 c = 4.380	a = 3.321 b = 10.613 c = 4.382	-42.5719
Pb	a = 4.805	a = 5.033	-14.2496

Table 6.1 (continued)

Pd	a = 3.890	a = 3.927	-20.7535
Sc	a = 3.309 c = 5.268	a = 3.307 c = 5.113	-12.2626
Si	a = 5.430	a = 5.445	-43.2992
Sn	a = 5.830 c = 3.175	a = 5.922 c = 3.220	-30.9074
Sr	a = 6.080	a = 6.013	-2.4904
Ti	a = 2.950 c = 4.683	a = 2.923 c = 4.632	-15.4650
Tl	a = 3.456 c = 5.539	a = 3.512 c = 5.607	-4.5012
V	a = 3.303	a = 2.988	-17.8116
Y	a = 3.647 c = 5.731	a = 3.613 c = 5.641	-12.8034
Zn	a = 2.665 c = 4.947	a = 2.656 c = 4.941	-2.2357
Zr	a = 3.232 c = 5.148	a = 3.209 c = 5.118	-16.9977

As to compare the experimental (taken from the Pearson's Handbook by Villars [62]) and calculated lattice constants of impurity elements, it is realized that both are quite close to each other. Comparison of the two in quantitative manners puts forth that the percent errors in lattice parameters a , b and c are generally *less* than the order of 2 %. More specifically, for hexagonal magnesium unit cell, the percent errors in calculation of the equilibrium lattice parameters a and c , relative to experimental values are; ~ 0.7 and 0.4 %, respectively. Consequently, it is revealed that errors on this order are quite a success for the pseudopotential method where no experimental data are used. Therefore, the strength in prediction of the stable systems by first principles calculations is verified once more.

The last column in Table (6.1) indicates the total energy values of the unit cell systems. As also seen from Eq. (5.2), fifteen moles of Mg and sixteen moles of H₂,

with one M atom to be substituted at the center of the tetragonal MgH₂; go into reaction in order to form the alloyed 3x3x3 magnesium hydride structure. On this basis, the unit cell system energies calculated should be divided by the number of M atoms present in that unit cell.

6.1.1 Hydride formation energies

The primary objective in calculating the formation energies for each system of MgH₂ is to systematically investigate the effect of alloying elements on the decrease in hydriding energies. As a matter of fact, what is desired is to attain alloyed structures with decreased (in absolute manner); but still negative formation energy values; so that the hydride in question would be thermodynamically stable. Since the experimentally explored characteristics of MgH₂ point out high desorption enthalpy and thus temperature, altering the chemical composition has become a conventional way of destabilizing Mg hydride [11,14,63].

Firstly, again the structural parameters for each alloyed magnesium hydride system were calculated and compared to the experimental values. In this regard, the equilibrium cell parameters *a* and *c* of pure MgH₂ were found to be 8.811 and 5.952 Å, respectively. Comparison shows us that; these calculated values are of 1.0 and 1.2 % different than the initially set experimental values, which is a strong implication of the good agreement between the computational and experimental results.

The results related to Mg hydride 2x2x2 supercell parameters, calculated total energies and formation energies are tabulated in Table (6.2), where numbers in parentheses are the experimental cell parameters for pure MgH₂ [62]. Total energies in eV represent the calculated internal energies for each system where $\Delta E_{\text{bulk(hyd)}}$'s in kJ/mol-H₂ were calculated via the hydride formation reactions. As also mentioned by Kinacı and Aydınol [64], formation energies are not exactly

the real formation energies due to the approximations used; therefore relative difference in the energies gains importance. It is useful to recall the hydride formation energy method once again:

$$\Delta E_{bulk(hyd)} = E_{Mg_{15}MH_{32}} - (15E_{Mg} + 16E_{H_2} + E_M) \quad (5.2)$$

Table 6.2 Cell parameters, total energies and formation energies of Mg hydrides

System	Cell Parameters a, c (Å)	Total Energy (eV)	$\Delta E_{bulk(hyd)}$ (kJ/mol-H ₂)
Pure	8.811, 5.952 (<i>exp: 8.901, 6.025</i>)	-142.5935	-72.0163 (<i>exp: -75.2</i>)
P	8.752, 6.015	-141.7219	-34.6751
K	8.908, 6.087	-138.2720	-39.7519
Tl	8.911, 5.997	-139.7576	-41.3475
Si	8.785, 6.002	-143.1381	-42.6663
Sn	8.885, 6.058	-141.7588	-43.6888
Ag	8.805, 5.976	-140.6589	-43.9764
Pb	8.915, 6.067	-141.5711	-44.3723
Au	8.807, 5.979	-141.2460	-44.6857
Na	8.818, 6.030	-139.3660	-44.7252
Mo	8.767, 5.941	-148.9621	-45.1457
Ge	8.838, 6.001	-142.6641	-45.2482
In	8.873, 5.999	-140.8471	-45.9638
Nb	8.794, 5.968	-148.6770	-47.3710
Cr	8.776, 5.929	-148.0653	-48.1433
Li	8.746, 5.972	-140.5752	-48.3449
Cu	8.805, 5.941	-142.4702	-48.6295
V	8.776, 5.939	-147.8483	-50.0025
Pd	8.769, 5.946	-144.1710	-50.2446
Mn	8.755, 5.913	-148.1413	-51.6184
Ni	8.809, 5.915	-144.7640	-52.1112
Al	8.768, 5.975	-142.9848	-52.2154
Hf	8.805, 5.999	-149.2120	-52.3252

Table 6.2 (continued)

Fe	8.832, 5.948	-147.6645	-52.5422
Cd	8.850, 5.967	-140.1537	-52.6785
Zr	8.819, 6.007	-148.0668	-53.7742
Co	8.765, 5.918	-146.6566	-54.0302
Ti	8.783, 5.960	-147.4430	-54.6338
Zn	8.806, 5.921	-140.9758	-55.5222
Y	8.784, 6.094	-147.0545	-60.3149
Sc	8.797, 6.008	-146.9030	-61.0321
Ca	8.856, 6.037	-143.5710	-66.2704
Sr	8.898, 6.097	-145.5478	-82.3215

We derived the energies of Mg and H₂ unit cells as -3.0157 eV and -6.7520 eV, respectively. From here, formation energies of the alloyed supercells were obtained for 32 different structures using Eq. (5.2). Afterwards, hydride formation energies were recalculated in kJ, on the basis of one mole of hydrogen molecule. Formation enthalpy of pure MgH₂ was obtained as -72.0163 kJ/mol-H₂ where the experimentally measured value by Bogdanovic et.al. [65] is -73.5 kJ/mole-H₂; which are very close to each other. Another supporting result for the enthalpy of formation of MgH₂ was proposed by Song et al. [10], which was calculated as -71.15 kJ/mol-H₂.

It is quite appealing that; all of the impurity elements doped in Mg hydride structure, except for Sr, make a contribution to the enthalpy of formation by means of decreasing its absolute value. The alloying elements are sorted in Table (6.2) according to a descending order in the effect of decreasing magnesium hydride formation energy. In this respect, *P, K, Tl, Si, Sn, Ag, Pb, Au, Na, Mo, Ge* and *In*, in the decreasing order, were found to be among the most favorable elements lowering the magnesium hydride formation energy. For instance, the decrease in hydriding energies could be expressed as ~ 37.3 and ~ 26.1 kJ/mole-H₂

for *phosphorus (P)* and *indium (In)* substituted systems respectively. Correspondingly, 31 out of 32 elements studied are expected to decrease the stability of magnesium hydride and ease the hydrogen desorption process. Furthermore, the study of Yazıcı and Aydınol [66] which investigates the effect of Ti and Al on MgH₂, support this conclusion by stating that both of these elements contribute to dehydrogenation thermodynamics. Finally, it should be stressed that; by leading to a decrease in the hydride stability, mentioned elements would be beneficial in creation of MgH₂ with improved hydrogen desorption properties.

6.2 Surface calculations on magnesium and magnesium hydride systems

In the succeeding part of this study, two different kinds of calculations on Mg and/or MgH₂ surfaces were performed; which are molecular dynamics simulations and ionic relaxations within the ab initio pseudopotential total energy methods. It was aimed to observe which one of the selected elements would be efficient, in terms of their abilities to dissociate hydrogen molecule and be adsorbed on the surface. In this regard, MD simulations on H₂/Mg (0001) interaction, charge density distributions, adsorption energy calculations (with dopants placed in different configurations) and work function calculations over alloyed Mg and/or MgH₂ surface structures were systematically investigated. Accordingly, the results are discussed in details in the following sections.

6.2.1 Molecular dynamics calculations

After completing the calculations regarding bulk Mg hydride and detecting the effects of alloying elements on hydride stability decrease; thus improvement in hydrogen desorption kinetics, the study has moved onto a different field which is the dynamic and total energy calculations on the surface of Mg. Firstly, via molecular dynamics simulations, what kind of an effect would the substitutionally placed impurity elements make on hydrogen behavior at the surface has been studied. To our knowledge, no such comprehensive first

principle molecular dynamics calculations for H₂ adsorption on magnesium surface have been performed so far, therefore our study is considered to be significant in this manner. In this section, outcome of the simulations executed on Mg (0001) surface will be explained and discussed.

Principally, the goal was to study dissociation and subsequent adsorption of hydrogen molecule at the surface for each alloyed structure. In another saying, we desired to see whether the substituted elements displayed an effect of *catalyzer* in terms of dissociation of the hydrogen molecule into H atoms at the surface. MD simulations were firstly executed on clean Mg (0001) surface (at the temperature in question, 300 K), within a limited simulation time. Even though the simulation continued for 10 ps, it was seen that the splitting of H₂ without any alloying addition is not possible, most probably due to the homogeneous charge distribution over the surface. Indeed, Sprunger and Plummer [17] have observed no dissociative chemisorption of H₂ on pure Mg (0001) surface (≥ 110 K), which is supported by the theoretical results implying the existence of a large activation barrier that H₂ must overcome to be dissociated (since the single s electron of H is tended to be repelled by Mg, due to the Pauli exclusion principle). Therefore, it is obvious that the interaction between Mg and H should be affected or predominated by the M - H interaction, thus leading to a decline in the activation barrier for hydrogen to be adsorbed on Mg (0001) surface.

In this respect, it is apparently necessary to dope some elements on magnesium surface in order to ease dissociation. In addition to the elements selected for bulk studies, Ru and Rh have also been chosen as the dopants. Simulation results revealed that systems alloyed with most of the transition metals are good at dissociating the hydrogen molecule.

According to the results of MD calculations, the thirty four elements studied were grouped into two, as also indicated in Fig. (6.1), in terms of their success in splitting the hydrogen molecule. Those which were able to retain the H-H

separation distance above 2-3 Å, once dissociation occurred, were classified as the *splitting (S)* elements. The second class is the *non-splitting (NS)* characteristic, where H-H distance is maintained nearly at its equilibrium value; which is less than 1 Å during the entire simulation time. While some non-splitting elements have no effect on the hydrogen action in vacuum, some are observed to repulse the hydrogen away from the surface to some extent; such as Cd, In and Zn. Although not studied extensively, the simulation executed for magnesium surface substituted with one oxygen atom supports the fact that hydrogen intake is inhibited by the oxygen presence at the surface [12]; since H₂ is found to be repelled from the surface in this case. In summary, one can say that; *3d* (from Ti to Ni) and *4d* (from Zr to Pd) transition metals are accomplished in catalyzing the hydrogen dissociation.

A further categorization among the splitting dopants puts forth the rate of adsorption of one of the hydrogen atoms on the surface. According to this, we suggest the two groups as such: rapid (*early*) adsorption in between 30 – 200 fs and relatively slower (*late*) intake of hydrogen after 200 – 500 fs. In the early group, Mn, Fe, Co and Nb induce the fastest hydrogen adsorption on surface within at most 70 fs, while for systems doped with Cr, Ni and Hf, it takes a little longer time for H to be attracted inside the slab of magnesium. For the transition metals other than the stated ones, which are; Ti, V, Zr, Mo, Ru, Rh and Pd, hydrogen adsorption occurs within 250 to 500 fs. Fig. (6.1) clearly exhibits the “S” and “NS” elements, according to their positions in the periodic table, as well as which one of the characteristics “E” or “L” are displayed by these elements.

Subsequently, outcome of the MD simulations were further analyzed by graphical means for each of the thirty four systems. In this respect, the distance between the hydrogen atoms and positions of either hydrogen (H1 and H2) in z direction are given with respect to the simulation time in Fig. (6.2) for ten representative systems, namely; unalloyed, silver, calcium, cobalt, iron, hafnium, manganese, niobium, titanium and zirconium doped magnesium surfaces. Fig.

(6.2(a)) shows clearly that the H₂ molecule is definitely not dissociated on pure magnesium surface; where in Fig. (6.2(b)), the unsplit H₂ molecule is observed to be in a fluctuating motion within the vacuum region. Similarly, Fig. (6.2(c)) and (6.2(e)) display the non-splitting behavior of Ag and Ca dopants, where in Fig. (6.2(d)) and (6.2(f)), it is seen that both hydrogens are oscillating above the surface, preserving the molecule state.

On the other hand, as could be seen from Fig. (6.2(g)), the distance between H atoms reaches above 3 Å, immediately after 50 fs in Co substituted surface; which implies the early adsorption of H by Co. Succeeding figures exhibit that; separation time of the H's from each other (to above 3 Å) is ~ 40, 150, 30 and 70 fs for surfaces substituted with Fe, Hf, Mn and Nb, respectively.

Besides these elements which are examples of early adsorption cases, Ti and Zr substituted surfaces are representatives of late adsorption, as in Fig. (6.2(q)) and (6.2(s)). For Ti doped Mg surface, separation at around 3 Å takes place after 250 fs, while the duration for Zr is seen to be 450 fs.

Moreover, as observable in Fig. (6.2(h)), (6.2(j)), (6.2(l)), (6.2(n)), (6.2(p)), (6.2(r)) and (6.2(t)), right after the decomposition of H₂, one of the H's is being adsorbed on the surface and drawn into the slab (horizontal line represents the position of the surface). For Co and Fe substituted surfaces, the second hydrogen is also seen to be penetrated through the surface at around 1300 and 3200 fs respectively, as seen in Fig. (6.2(r)) and (6.2(t)). The simulation regarding Co as the dopant displays that; once both are adsorbed on the surface, one of the hydrogens is attracted even more into the lattice where the other maintains its position around the surface. In the meantime, separation distance of H's is being kept above 3 Å. On the other hand, in Fe substituted case, both H's continue being around the vacuum-substrate interface.



Figure 6.1 Trends in hydrogen dissociation through alloying elements

However, unlike the situation for Co and Fe, the second H atom does not proceed inside the adsorbent for Hf, Mn, Nb, Ti and Zr doped systems (as far as we can observe within the limited simulation time). Finally, it is worth mentioning that, a separation of 3 Å could be considered as a criterion for full decomposition of the hydrogen molecule.

In correlation with this study, several other theoretical and experimental studies [12,13,16,67] put forward the efficiency of $3d$ and $4d$ transition elements in general, in terms of the catalysis of H_2 dissociation, relating to their orbital occupancies. More specifically, Du *et. al.* [68,69] via the nudged elastic band method (NEB), have stressed the effectiveness of Ti and Pd as catalysts on the decrease in activation barrier for H_2 adsorption. Moreover, Pozzo *et. al.* [21] detected the improvement of H_2 intake kinetics through Mg surface, via doping Ni and Ti as the adsorbates, where the interaction of their unfilled d orbitals and s electron of hydrogen is seen to be predominant over Mg - H bonding.

As a further remark we should state that; at first sight, each of the fourteen elements seems to achieve the catalyzer effect on H_2 dissociative adsorption. However, it is more pronounced specifically for the middle transition metals, whereas for the early and late transition metals the effect is somewhat delayed. Although middle transition metals generally have no or less stable binary hydrides [70,71], therefore less affinity to hydrogen, when alloyed on Mg surface they have a strong influence on H_2 dissociation.

Apart from the molecular dynamics studies performed on magnesium surface, charge density difference distributions on $(\bar{2}110)$ plane of Mg were computed for each alloyed structure in order to depict the mechanism behind splitting of the hydrogen molecule, in terms of the effects of added elements. The difference of the charge densities were taken between the final relaxed cell of the alloyed one and pure Mg cell having the same volume and atomic configuration; so that

it could be possible to take the difference point by point and investigate the charge dispersion around the adsorbates, from the dopant-effect point of view.

We assessed several characteristic behaviors of charge densities, some representative examples of which are as illustrated in Fig. (6.3), relying on the positions and grouping of the adatoms in periodic table. According to this, an interesting behavior came out to be the spherical symmetry in accumulation of electrons around the adsorbed elements, which are Ag, Au, Cd, Cu, P, Tl and Zn. Another characteristic attribute is exhibited by Al, Ge, In, Pb, Si and Sn doped surfaces; where there is again a spherical denseness of electrons, however with lower charge values and a distorted spherical shape this time. Contrarily to the situations mentioned above, electron depletion instead of accumulation is observed at the center site of magnesium-vacuum interface, for alkaline metals such as Li, Na, K, Ca and Sr. Among these alkaline elements, Na exhibits the depletion effect most obviously. Moreover, K, Ca, Sr and Li also seem to have dispersed their charges to the surroundings.

Selective illustration of the charge density differences introduces the common behavior of hydrogen-dissociating elements (as shown in Fig. (5.3)), which is the effective and oriented increase in electron density at the adsorbent-adsorbate interface. More specifically, elements such as Co, Cr, Fe, Mn and Ni display an important characteristic which is the upwards-oriented branches, aligned towards a direction in between the neighboring surface Mg atoms, in a 6-fold like symmetry. The rapid dissociation of hydrogen molecule and immediate attraction of one of the hydrogen atoms inside the lattice could be attributed to this configuration, especially for Co, Fe and Mn elements. On the other hand, charge density difference plots for some of the late adsorbing surfaces are appealing, in terms of their rather spread and flat electron density distributions at the branches.

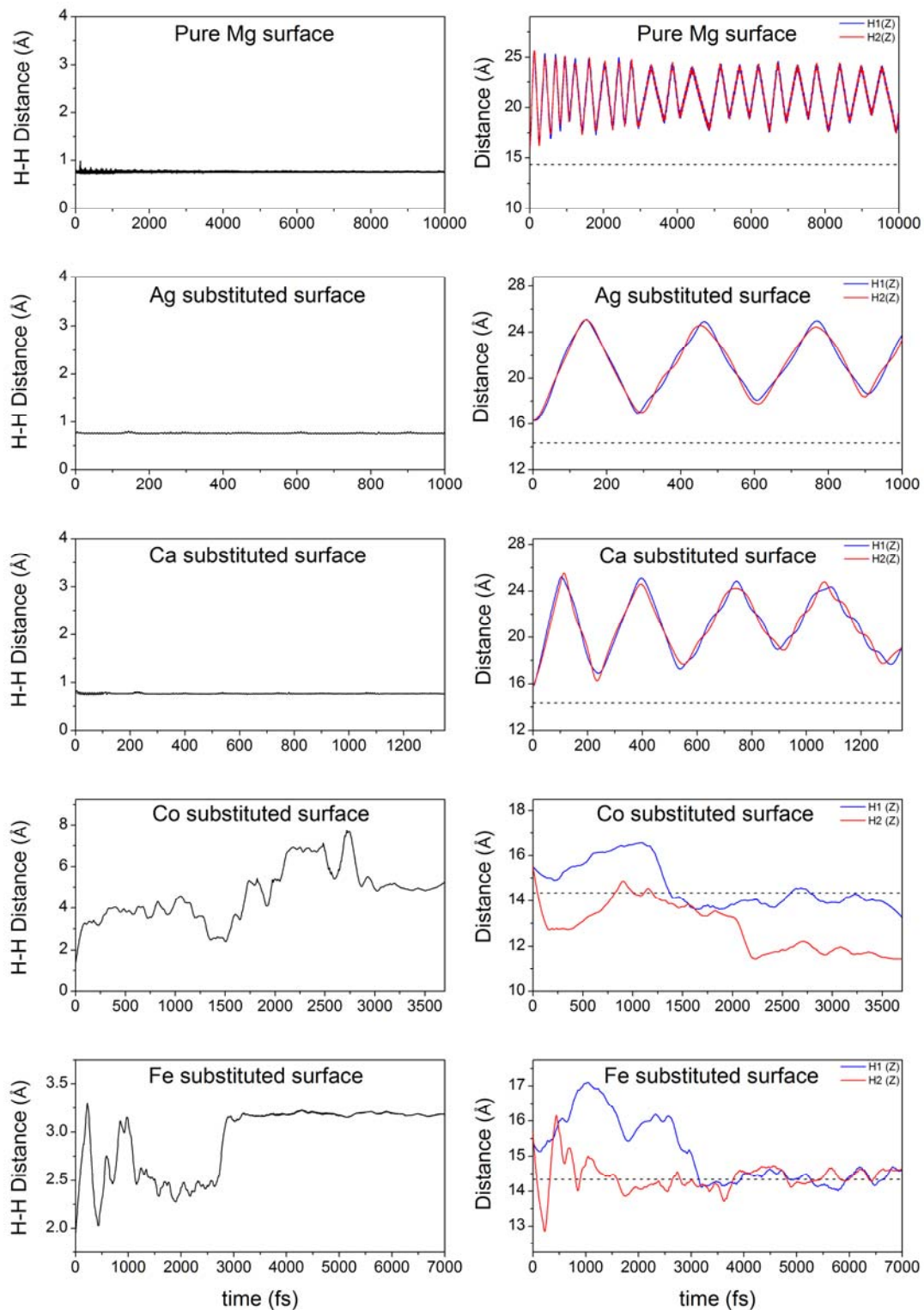


Figure 6.2 The variation of separation between H atoms and z coordinates of either H atom throughout the simulation for the mentioned surface structures

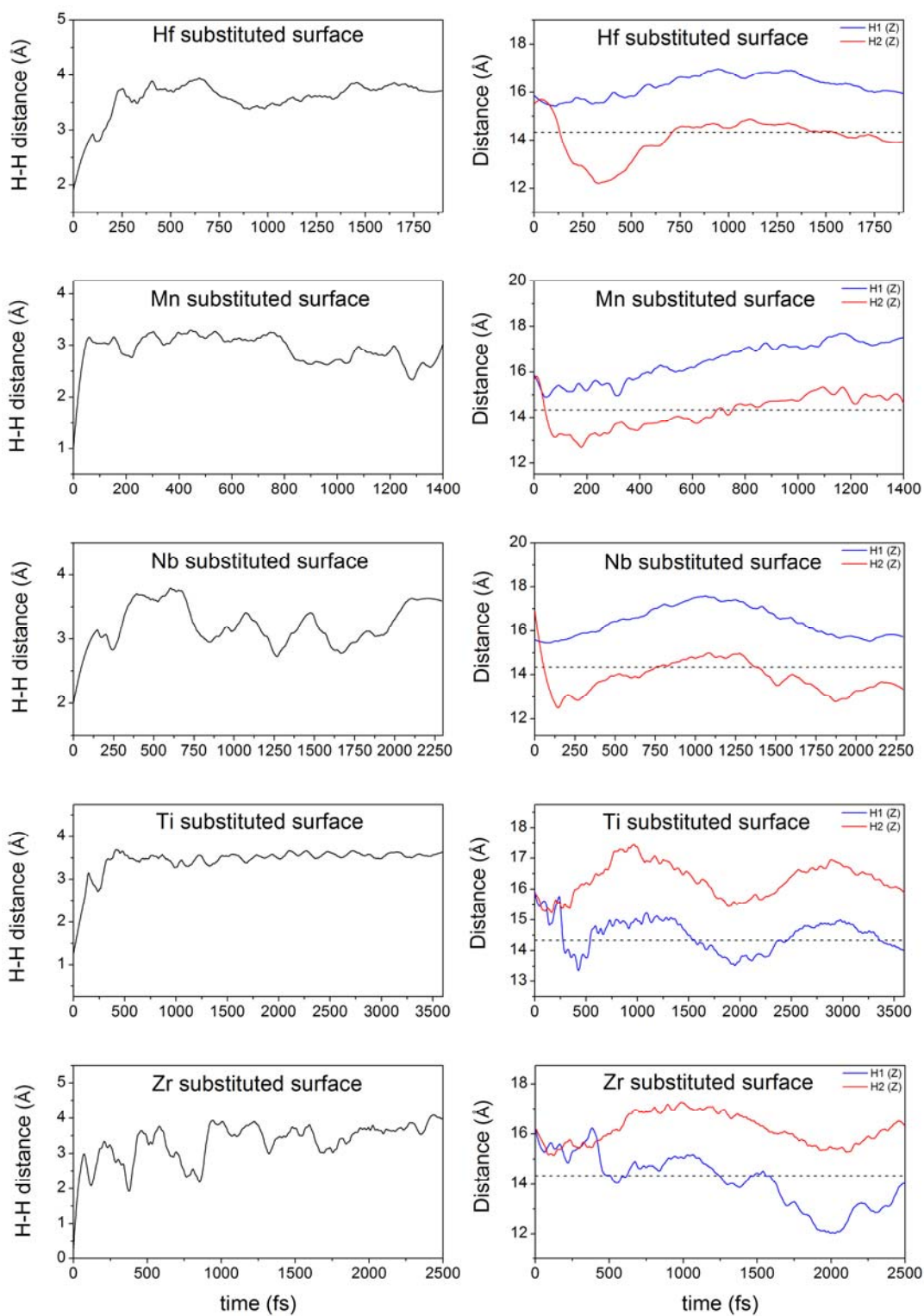


Figure 6.2 (continued)

Fig. (6.3) presents samples from each of the characteristic groups. For instance, Ag, Cd and Tl are examples of the elements exhibiting nearly spherical symmetry around the dopant; which represents the non-splitting behavior. Furthermore, Al, Pb and Sn stand for again the non-splitting elements, with a relatively distorted symmetry around the adatom. Also, Ca, Li and Na doped surfaces exhibit a configuration in which the obvious charge depletion around these adsorbates could be treated as a reflection of the agreement between charge density difference plots and non-splitting characteristic of the alkaline elements. On the other hand, Co, Cr, Fe, Mn and Ni represent the fast adsorbing hydrogen splitting elements with the mentioned upwards-oriented branches in a 6-fold like symmetry, pointing towards the neighboring Mg atoms. Finally, illustrations regarding the Ti, V and Zr doped surfaces are representative examples of the late adsorbing splitting elements. The relatively dispersed and flat distribution of electronic density at the surface is quite apparent in the figure.

A more detailed visualization of the upwards-oriented branches of the electronic density difference for fast adsorbing and flat distribution for late adsorbing surfaces is as displayed in Fig. (6.4), for surfaces substituted with Co and Zr. These isosurfaces of charge density differences, taken at the alloying element site and computed at 0.1 eu, clearly show the difference in the surface electronic state between the early and late hydrogen adsorbing surfaces, in terms of the characteristic H_2 dissociation behavior.

In light of the MD simulation results and charge density difference plots regarding magnesium surface, a general conclusion is reached. To summarize, the impurity elements which were seen to be effective in *catalyzing H_2 dissociative adsorption* at the surface, also display a distinct configuration of charge dispersion around the surface-vacuum interface. The upwards-oriented branches could be considered as to attract the hydrogen molecule and serve in its rapid dissociation into H atoms. Correspondence in between is seen to verify the strength of

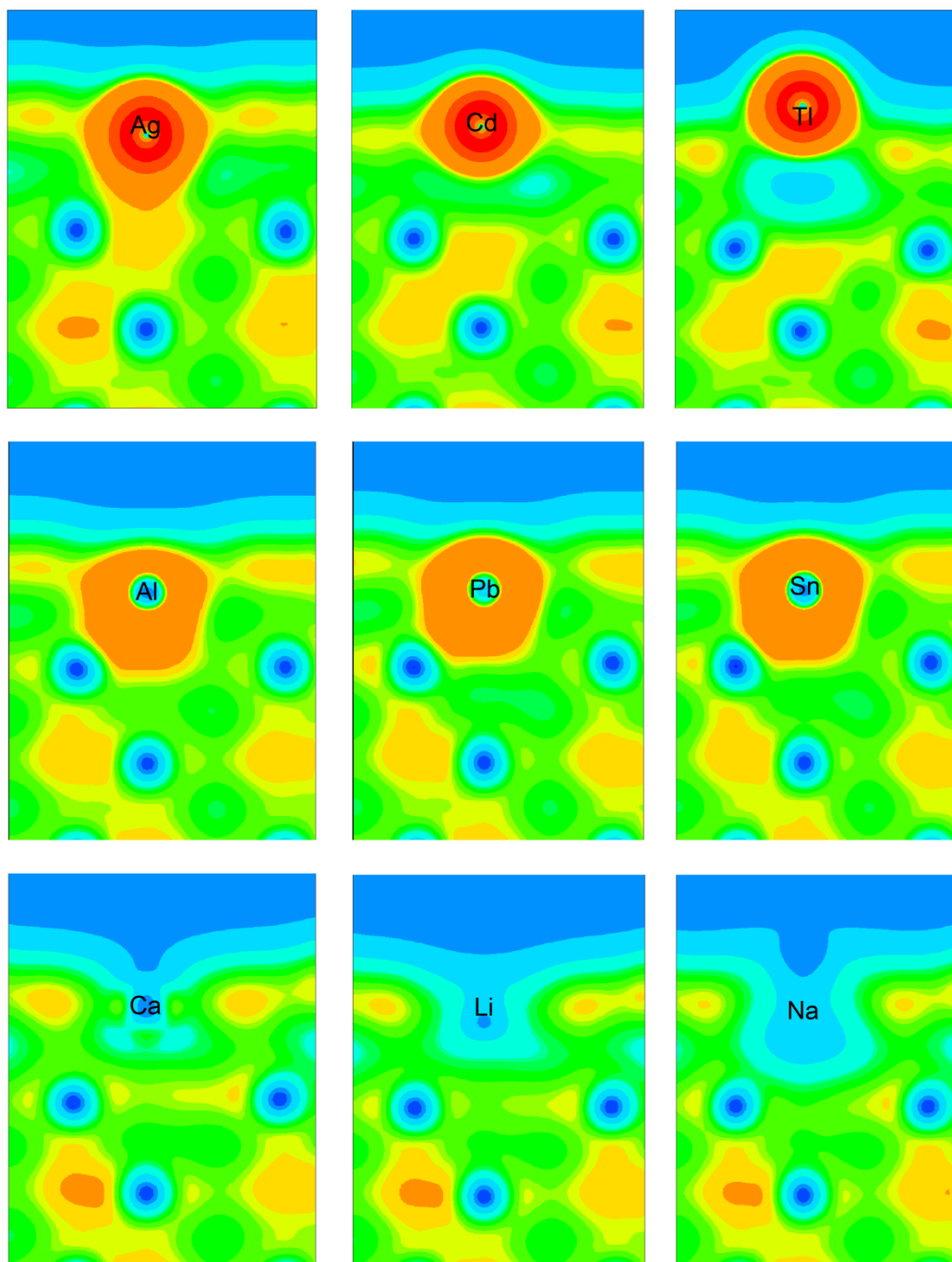


Figure 6.3 Charge density difference illustrations of the selected Mg surface structures

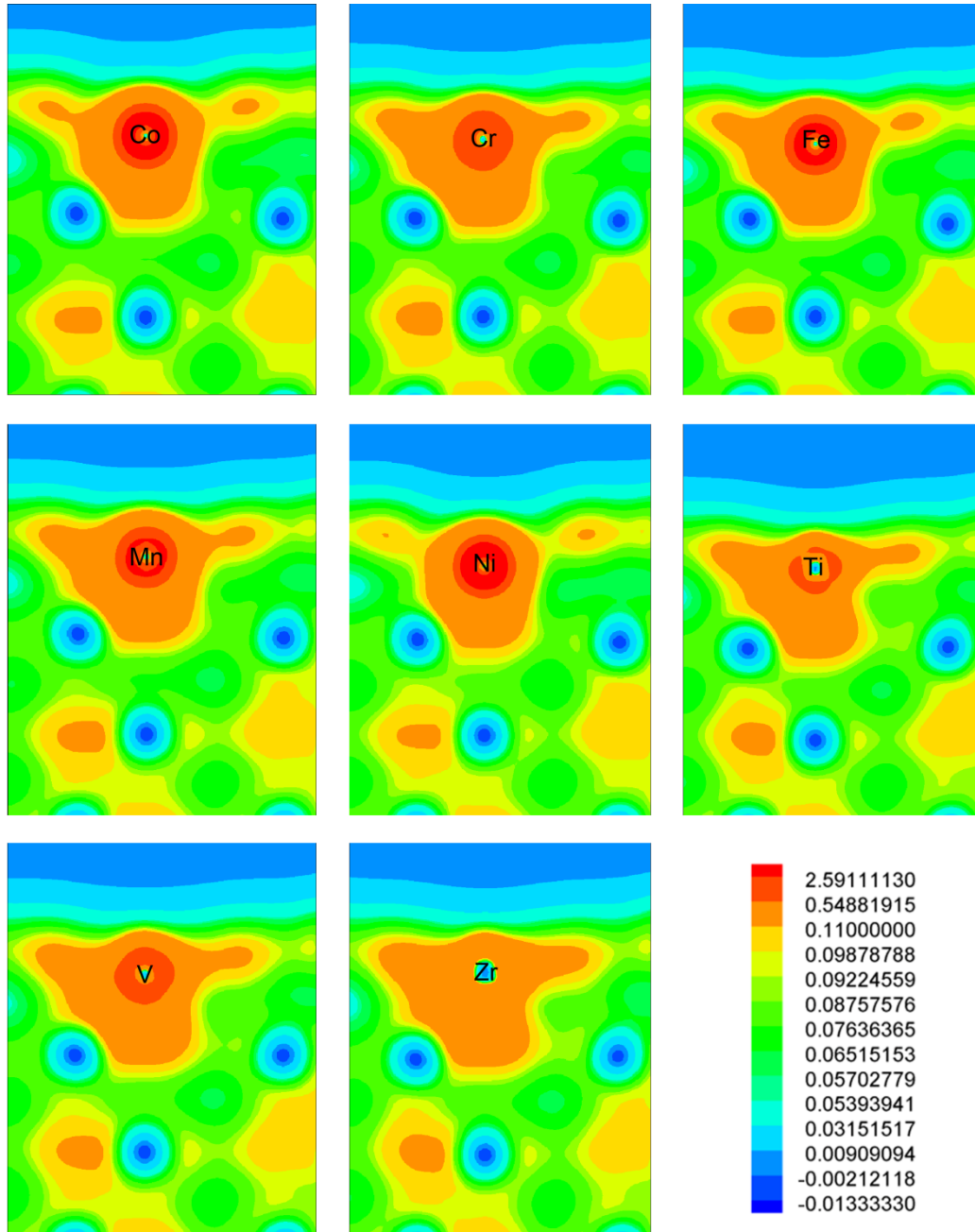


Figure 6.3 (continued)

especially middle $3d$ transition elements in the early dissociative adsorption of hydrogen.

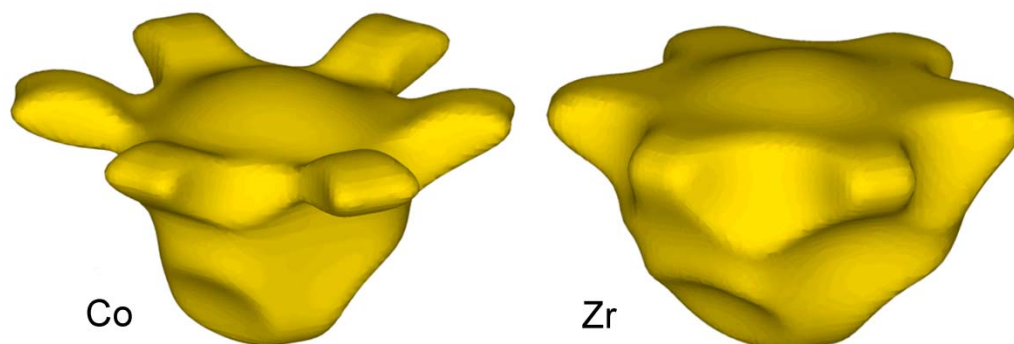


Figure 6.4 Isosurfaces of charge density difference taken at the alloying element site for magnesium surface structures alloyed with Co and Zr elements

6.2.2 Ionic relaxations on surface structures

This study covers a final major set of total energy calculations; which were executed on Mg hydride (001) and mostly on Mg (0001) surface structures. In this regard, adsorption phenomenon has been studied for the impurity elements in question; with the urge of elucidating the interaction between adsorbates and the substrate. Via calculation of the adsorption energies on Mg and MgH₂ surfaces for different configurations, it was aimed to seek for the preferred site of adsorption of the dopants. Furthermore, work function calculations on Mg (0001) surface systems doped with the previously mentioned impurity elements were performed.

6.2.2.1 Substitutional adsorption on magnesium (0001) and magnesium hydride (001) surfaces

Firstly, adsorption of the adatoms substituted on magnesium and magnesium hydride surfaces has been investigated within the context of surface alloying studies. As may be recalled, selected elements were doped in four different positions. First one is the center of uppermost layer of substrate, where the alloying element is substituted instead of a magnesium atom (as could be seen from Fig. (6.2) and (6.3)). Therefore, this phenomenon of the element occupying topmost center site is surface-substitutional adsorption. Corresponding adsorption energy calculation methods were explained previously, as in Eq. (5.3) and (5.4). In order to remember once again:

$$E_{sub-ads,Mg(0001)} = E_{M/Mg(0001)} - E_{Mg(0001)} - E_{M-atom} + E_{Mg-vacuum} \quad (5.3)$$

$$E_{sub-ads,MgH_2(001)} = E_{M/MgH_2} - E_{MgH_2(001)} - E_{M-atom} + E_{Mg-vacuum} \quad (5.4)$$

As a result of the surface ionic relaxations, energy of pure magnesium surface structure was obtained as -68.8922 eV, and that of Mg atom at the kink site in vacuum as -0.5991 eV. Knowing the total energies of alloyed Mg (0001) surfaces and free energies of the corresponding adatoms, substitutional adsorption energies could be calculated. In addition, total energy of the unalloyed surface structure of Mg hydride was found to be -463.189 eV, and that of Mg at the kink site, above MgH₂ surface, as -0.2797 eV. Here again, with all the information attained, substitutional adsorption energy for doped MgH₂ systems have been calculated.

Corresponding results of the adsorption energy calculations for substitutionally alloyed Mg (0001) and MgH₂ (001) surfaces, represented by $E_{sub-ads,Mg(0001)}$ and $E_{sub-ads,MgH_2(001)}$ respectively, are tabulated in Table (6.3) for every single system. Accordingly, the results display that all of these thirty two elements would be adsorbed on Mg surface (in terms of their negative adsorption energies).

Examination of the values in more detail reveals that; elements acquiring the potential of being adsorbed on substrate Mg more extensively with respect to the others are; *Mo, Nb, Cr, Mn, Fe, V, Zr, Hf, Co, P, Ti* and *Ni* respectively. Surface-substitutional adsorption energies of the mentioned species vary between -9.2626 (*Mo*) and -5.2995 eV (*Ni*). On the other hand, the highest energy value is that of Cd within all elements, which was found as -0.5628 eV, implying the lowest chance of adsorption, relative to other adatoms.

On the other hand, calculations regarding the substitutionally doped MgH₂ (001) surface systems point out that; dopants *other than Zn, Au, In, Ag, Li, Tl, Cd, Na* and *K* would be adsorbed on the magnesium hydride surface. Here in this case, the elements holding relatively higher probabilities of adsorption on Mg hydride surface, in a descending order, came out to be: *Fe, Mn, Mo, Cr, Co, Nb, V* and *Ni*. Corresponding substitutional-adsorption energies were derived as -6.1371 (*Fe*) and -4.3469 eV (*Ni*).

Furthermore, an interesting remark attained from the ionic relaxations performed on substitutionally alloyed magnesium surface is the correlation between the final configurations of atoms and adsorption energy values. More specifically, it was observed that; elements such as *Mo, Cr, Mn* etc. tend to be attracted inside the lattice for systems with lower adsorption energies, whereas dopants such as *Cd, K, Na* etc. within systems having higher energies (thus lower chance of adsorption) are elevated in the vacuum region to an extent.

6.2.2.2 On-surface adsorption on Mg (0001) surface

We have further continued surface alloying studies with the on-surface adsorption energy calculations, performed on only magnesium surface. The adatoms in this case are placed in three different positions which are; hollow, top and bridge sites (see Fig. (5.4)). In this case, since the elements are located at a finite distance to the surface; adsorption of these species to the surface is named as *on-surface* or *normal* adsorption. In this respect, normal adsorption energies of

each system, represented by $E_{nor-ads,Mg(0001)}$, were calculated via Eq. (5.5) for each of the three sites. The route of calculation, which is simpler relative to the substitutional case, may be recalled as:

$$E_{nor-ads,Mg(0001)} = E_{M/Mg(0001)} - E_{Mg(0001)} - E_{M-atom} \quad (5.5)$$

We already know the energy of pure Mg surface structure, which is -68.8922 eV and the free energies of adsorbates in question. Therefore, deriving the total energies of doped Mg (0001) surfaces, normal adsorption energies could be calculated.

Accordingly, that which one of the sites yields the most negative energy (in other words; the site of preference for adsorption of the doped species) was determined and tabulated as in Table (6.3), with initials indicated in parentheses. The results here again point out that; every dopant would be normally adsorbed on magnesium substrate. Similar to the consequence arisen from substitutional adsorption; *Mo, Nb, Mn, Co, Cr, Fe, V, P* and *Ni* are among the adatoms with increased probabilities of adsorption, where energy values are in the range of -9.2706 (*Mo*) and -5.2916 eV (*Ni*). *Cd*, on the other hand, possesses the highest on-surface adsorption energy, which is -0.912 eV.

Upon further examination of the results, see Fig. (6.5), it is seen that, for eighteen of the Mg surface structures, relatively lower adsorption energies are provided by bridge sites, for eleven of them by hollow sites, where only three of the systems are provided with lower values by top sites. Although there are groups of elements where predominantly bridge or hollow sites are preferred for adsorption, it is seen to be difficult to define a certain trend within the periodic table. Moreover, some inferences made from the final configurations are; besides the obvious or slight shifts of adatoms in the z direction, elements inserted in top positions generally seem to repulse the atom just underneath it towards the lattice, while itself is elevated in the vacuum to some extent. Another observation

is about the Mn and Mo elements, that is; they lead to an apparent dispersion of the top layer atoms.

A final remark should be made on the comparison of substitutional and on-surface adsorption energy results. Fig. (6.6) displays the sites of preferences for adsorption of the dopants on Mg (0001) surface, over each other. Among the transition metals, there has been detected a systematic in the way that; elements including and to the left of VIA column in the periodic table prefer to be adsorbed on substitutional sites (over hollow sites), while the transition elements to the right of VIA elements, with some exceptions, generally have the tendency to be adsorbed on bridge sites.

6.2.2.3 Work-function calculations

As an extension of the adsorption studies, work-function (Φ) values on alloyed Mg (0001) surfaces were calculated. As may be recalled, the work-function phenomenon is used to measure the minimum energy required to extract an electron from the Mg substrate, in this case. Accordingly, the value for pure magnesium surface was found to be 3.5515 eV. Results are indicated in Fig. (6.7) and Table (6.3), as in the form of difference between alloyed and pure surface states.

Monitoring the correlation between adsorption studies, charge density distributions and work-function calculations helps verification of the results obtained from adsorption energies and charge density difference illustrations. In this regard, the first remark to be made could be on the apparently low $\Delta\Phi$ for alkaline elements; Li, Na, K, Ca and Sr. It is seen that; these are among the dopants leading to a decrease in WF of pure Mg surface, where this implication of lower energy requirement (relative to the pure state) to remove an electron from the surface unravels the electron depletion around alkalines. On the contrary, among the elements yielding higher $\Delta\Phi$ values, there are Al, Si, Ge and

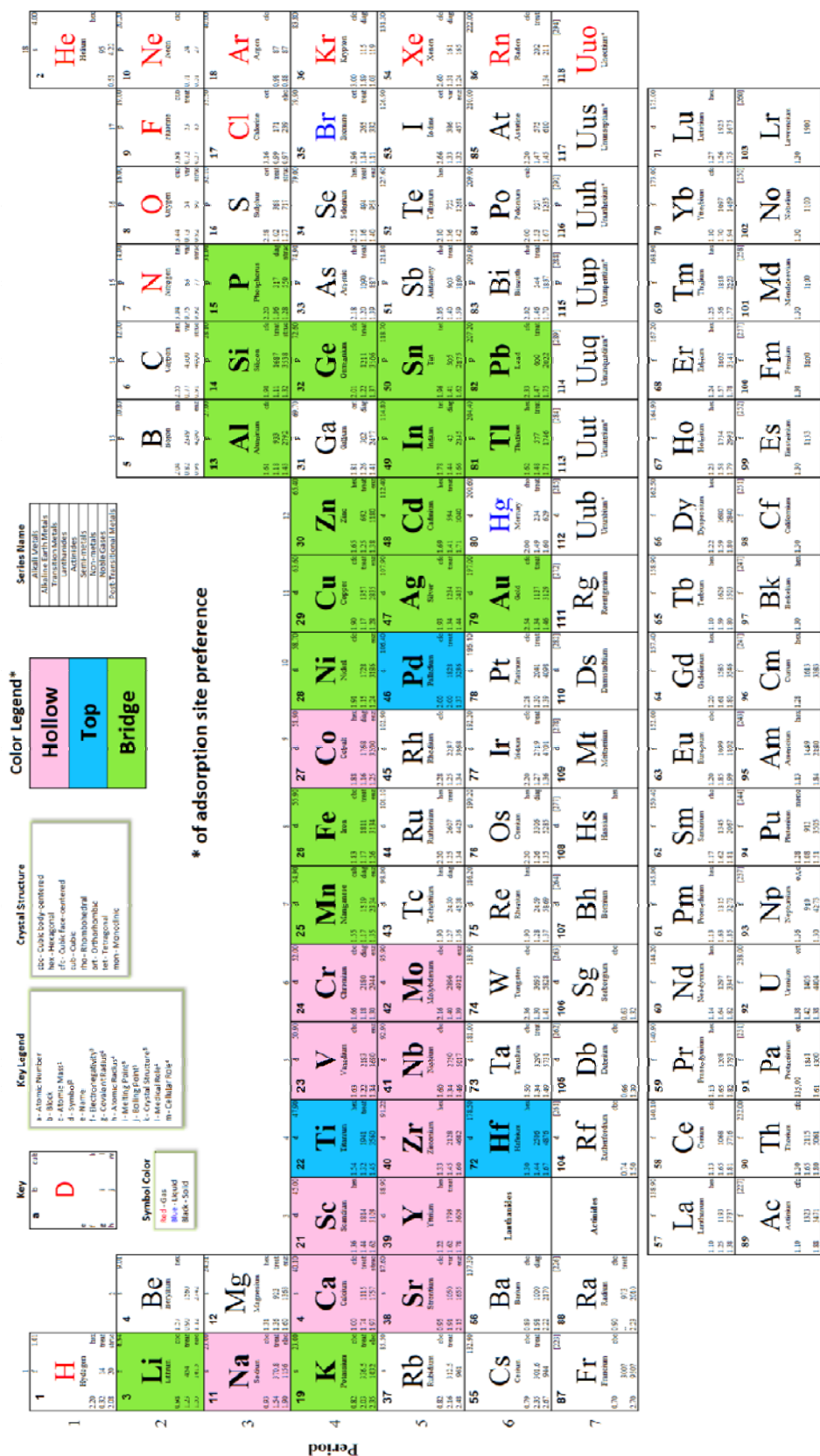


Figure 6.5 Sites of preference for normal adsorption on Mg (0001) surface

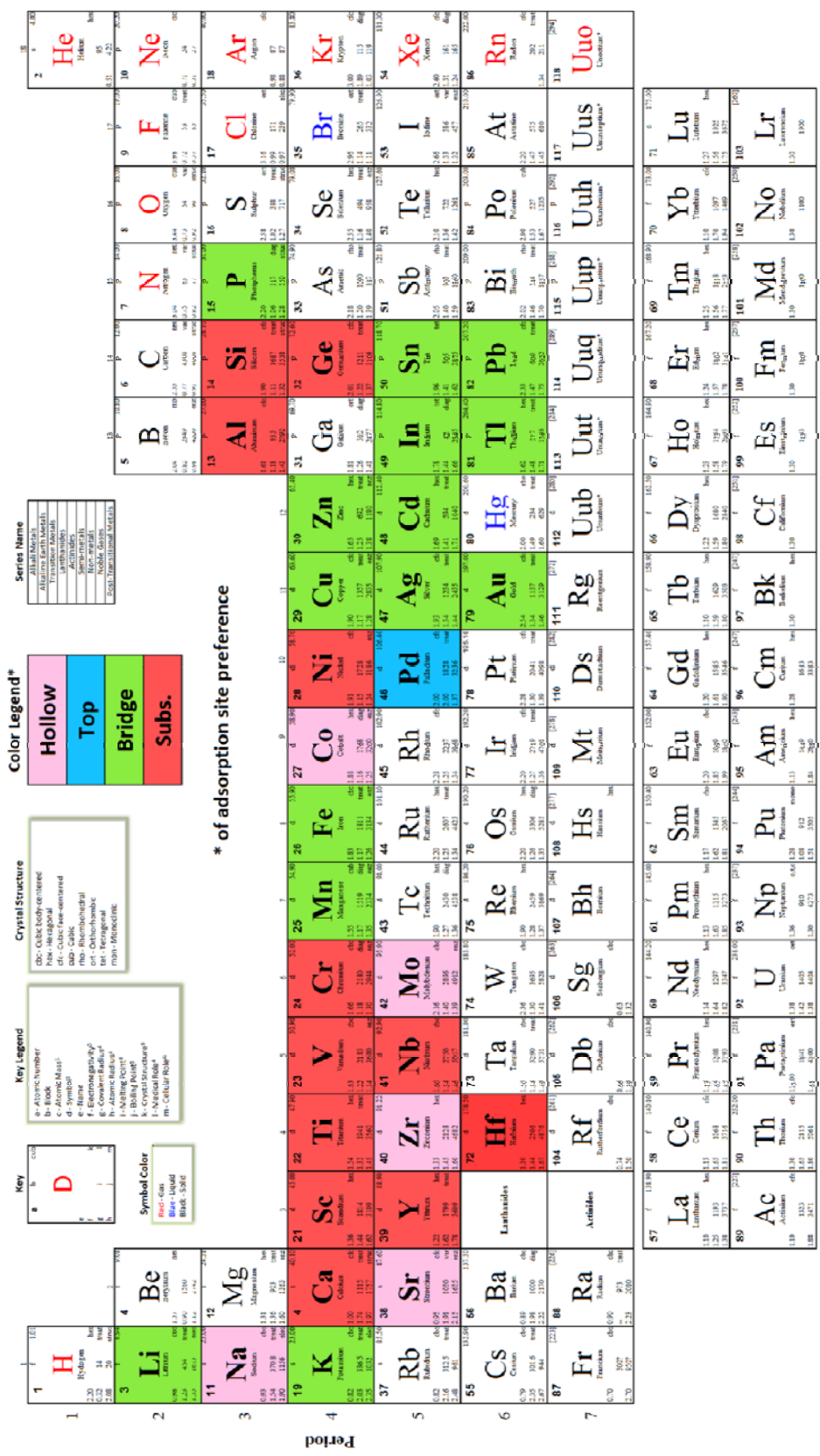


Figure 6.6 Sites of preference for adsorption on Mg (0001) surface

Tl. The electron density difference results are verified once more, since a spherical symmetry of charges around the mentioned elements (without any oriented branches) was seen to be created. Moreover, systems doped with elements from Ti to Zn seem to hold an average $\Delta\Phi$ of 0.033 eV, with the exceptions of Co, Ni and Cu. The similar trend is observed within the systems doped with Zr - Pb, except for the elements Pd, Ag, Cd and Tl, as could be seen from the related figure and table.

In summary, despite the existence of some exceptions, as a general trend most elements that tend to be adsorbed on the surface are seen to yield increased WF values. To put in other words, $\Delta\Phi$ values of which are generally positive also yield more negative substitutional or normal adsorption energies. On the other hand, it was observed that; dopants which have less affinities to bind to the Mg surface lead to decreased work-function values.

Finally, results achieved related to the surface calculations are summarized in Table (6.3). Systems are sorted according to their atomic numbers, in the increasing order. In the second column, outcome of the molecular dynamics simulations are expressed by the letters "S" (splitting elements) and "NS" (non-splitting elements), as well as the expression of early or late adsorption, by "E" and "L". Additional to the MD results tabulated, catalyzer effects of Ru (S, L) and Rh (S, L) elements should also be mentioned. Substitutional adsorption energies of the alloyed Mg (0001) and MgH₂ (001) surfaces are indicated in columns number three and four. In addition, on-surface adsorption energies and $\Delta\Phi$ values regarding magnesium surface doped with the 32 elements studied are as stated in the columns number five and six, respectively. All energies are given in terms of eV.

Table 6.3 Summary of the results of surface calculations, with energies in eV

Dopant	MD	$E_{\text{sub-ads,Mg(0001)}}$	$E_{\text{sub-ads,MgH2(001)}}$	$E_{\text{nor-ads,Mg(0001)}}$	$\Delta\Phi$
Pure	NS	-	-	-	-
Li	NS	-1.4426	1.3732	-1.7091 (B)	-0.0844
Na	NS	-0.9249	2.2768	-1.2978 (H)	-0.2602
Al	NS	-2.8573	-1.1102	-2.8290 (B)	0.0624
Si	NS	-4.8953	-2.5662	-4.6039 (B)	0.0563
P	NS	-6.1820	-1.4335	-6.2662 (B)	0.0231
K	NS	-0.7052	2.3435	-1.3025 (B)	-0.5413
Ca	NS	-1.6708	-1.3106	-1.3743 (H)	-0.1150
Sc	NS	-4.4122	-2.2925	-2.7642 (H)	-0.0280
Ti	S, L	-5.7472	-3.0307	-3.7261 (T)	0.0340
V	S, L	-6.8671	-4.4498	-6.2998 (H)	0.0332
Cr	S, E	-7.5106	-5.5632	-7.4238 (H)	0.0375
Mn	S, E	-7.5063	-5.9046	-7.7339 (B)	0.0336
Fe	S, E	-7.0414	-6.1371	-7.3799 (B)	0.0302
Co	S, E	-6.2140	-4.9816	-7.4789 (H)	0.0098
Ni	S, E	-5.2995	-4.3469	-5.2916 (B)	0.0080
Cu	NS	-3.072	-1.2367	-3.2239 (B)	0.0133
Zn	NS	-0.6010	0.1849	-0.9770 (B)	0.0283
Ge	NS	-4.4386	-1.8120	-4.2877 (B)	0.0580
Sr	NS	-1.2212	-1.3349	-1.2513 (H)	-0.1361
Y	NS	-4.5639	-2.4357	-2.8338 (H)	-0.0698
Zr	S, L	-6.8608	-3.5707	-4.6825 (H)	0.0118
Nb	S, E	-8.3449	-4.6551	-8.2461 (H)	0.0346
Mo	S, L	-9.2626	-5.6705	-9.2706 (H)	0.0438
Pd	S, L	-4.6656	-1.4628	-4.6930 (T)	-0.0243
Ag	NS	-2.6550	1.1780	-2.8060 (B)	0.0037
Cd	NS	-0.5628	1.4451	-0.9120 (B)	0.0119
In	NS	-1.8208	0.6247	-2.2433 (B)	0.0432
Sn	NS	-3.3616	-1.2689	-3.5007 (B)	0.0376
Hf	S, E	-6.3668	-3.1866	-3.8109 (T)	0.0314
Au	NS	-3.8270	0.2809	-4.0928 (B)	0.0139
Tl	NS	-1.8947	1.4301	-2.6318 (B)	0.0705
Pb	NS	-2.8062	-0.8597	-3.2776 (B)	0.0158

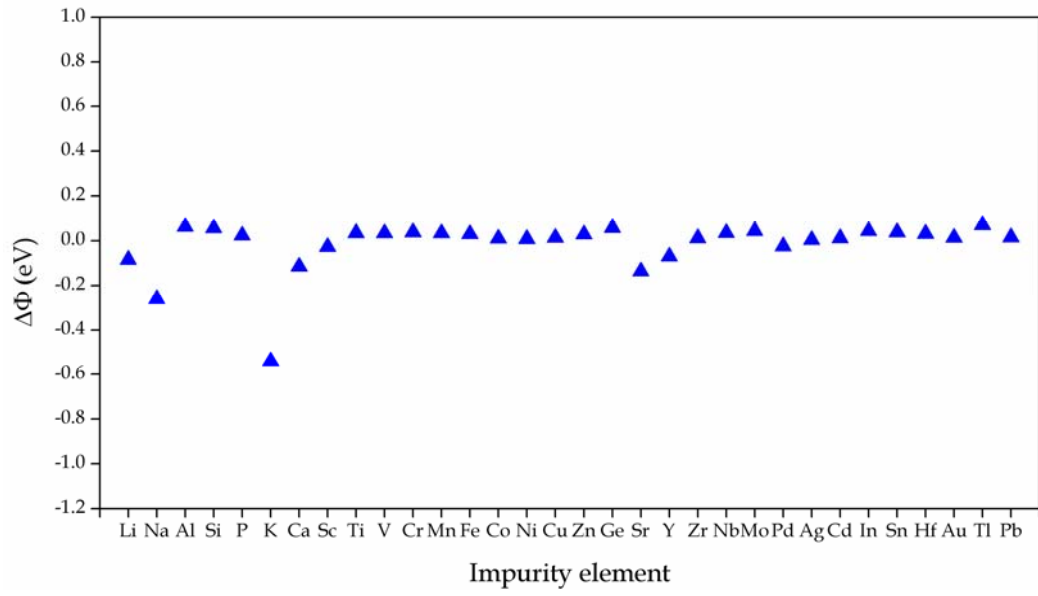


Figure 6.7 $\Delta\Phi$ values of substitutionally alloyed Mg (0001) surfaces

CHAPTER 7

SUMMARY & CONCLUSION

After testing the total energy package VASP for accuracy of theoretical predictions by comparing the calculated and experimental lattice constants, formation energies of several alloyed magnesium hydrides were calculated. What has come out of these calculations is that; hydrides alloyed particularly with *P, K, Tl, Si, Sn, Ag, Pb, Au, Na, Mo, Ge* and *In*, in the decreasing order, were found to attain decreased formation energies. Specifically, the decrease in hydriding energies could be expressed as ~ 37.3 and ~ 26.1 *kJ/mole-H₂* for *phosphorus (P)* and *indium (In)* substituted systems respectively. In addition, 31 out of 32 elements were expected to decrease the stability of MgH₂ and therefore the hydrogen desorption temperature.

In the next part of this study, calculations moved into different fields; which are the total energy and molecular dynamics computations over magnesium hydride and predominantly magnesium surfaces. Outcome of the MD simulations showed that a major part of *3d* and *4d* transition metals were accomplished at fulfilling a mission of catalyzer in terms of H₂ dissociation into its H atoms at the (0001) surface of Mg. Some elements were observed to dissociate hydrogen immediately; such as Mn, Fe, Co and Nb; whereas some other (e.g. Cr, Ni and Hf) gave rise to relatively delayed dissociation and adsorption cases. Charge density difference plots provided some ideas about why certain alloying elements on the surface enhance the adsorption of hydrogen. More specifically,

especially for Co, Mn and Fe elements, a correspondence may be monitored between the outcome of electronic density distributions and MD simulations; which display the rapid dissociation of H₂ and immediate attraction of one of the H atoms.

Moreover, substitutional and on-surface adsorption studies of the selected impurity elements revealed that elements such as Mo, Nb, Mn, Cr, Co, Fe, V, P, Ni etc. seem to possess higher probabilities of adsorption on the magnesium surface. A further interesting observation is on the systematic behavior in periodic table; elements included in and to the left of VIA column prefer to be adsorbed on substitutional sites (over hollow sites), while the transition elements to the right of VIA elements, generally have the tendency to be adsorbed on bridge sites.

A final remark could be on the correlation between the experimental results and theoretical calculations in this study, where in terms of catalysis, the power of *3d* and even *4d* transition metals; as stressed several times were verified. Although the slow adsorption/desorption kinetics of hydrogen still remains as a problem to be solved in practice, we hope that this study will guide some experimental approaches towards the effect of catalysis.

REFERENCES

- [1] W. Fulkerson, R.J. Judkins and M.K. Sanghvi, *Sci Am* **263** (1990) 129
- [2] L. Schlapbach, A. Züttel, *Nature* **414** (2001) 353
- [3] A. Züttel, A. Borgschulte, L.Schlapbach, *Hydrogen as a Future Energy Carrier* (2008) Wiley-VCH
- [4] M. Perruzini and R. Poli, *Recent Advances in Hydride Chemistry* (2001) Elsevier B.V.: A.J. Maeland, Chapter 18 – Hydrides for Hydrogen Storage 531
- [5] D. Ivey, D.O. Northwood, *J Mater Sci* **18** (1983) 321
- [6] L. Schlapbach, (ed.) *Hydrogen in Intermetallic Compounds I. Electronic, Thermodynamic and Crystallographic Properties, Preparation*. Topics in Applied Physics **63** (1988) Springer
- [7] A. Züttel, *Mater. Today* **9** (2003) 24
- [8] H.M. Jin, P. Wu, *Appl Phys Lett* **87** (2005) 181917
- [9] M.E. Arroyo y de Dompablo, G. Ceder, *J Alloy Compd* **364** (2004) 6
- [10] Y. Song, Z.X. Guo and R. Yang, *Phys Rev B* **69** (2004) 94205
- [11] T. Vegge, L.S. Hedegaard-Jensen, J. Bonde, T.R. Munter, J.K. Nørskov, *J Alloy Compd* **386** (2005) 1
- [12] A. Zaluska, L. Zaluski, J.O. Ström-Olsen, *J Alloy Compd* **288** (1999) 217
- [13] R. Baer, Y. Zeiri, R. Kosloff, *Phys Rev B* **55** (1997) 10952
- [14] G. Liang, J. Huot, S. Boily, A. Van Neste, R. Schulz, *J Alloy Compd* **292** (1999) 247

- [15] W. Oelerich, T. Klassen, R. Bormann, *J Alloy Compd* **315** (2001) 237
- [16] M. Dornheim, S. Doppiu, G. Barkhordarian, U. Boesenberg, T. Klassen, O. Gutfleisch and R. Bormann, *Scripta Mater* **56** (2007) 841
- [17] P.T. Sprunger, E.W. Plummer, *Chem Phys Lett* **187** (1991) 559
- [18] D.M. Bird, L.J. Clarke, M.C. Payne, I. Stich, *Chem Phys Lett* **212** (1993) 518
- [19] P. Ravindran, P. Vajeeston, R. Vidya, H. Fjellvåg, A. Kjekshus, *J Power Sources* **159** (2006) 88
- [20] T. Vegge, *Phys Rev B* **70** (2004) 35412
- [21] M. Pozzo, D. Alfè, A. Amieiro, S. French, A. Pratt, *J Chem Phys* **128** (2008) 94703
- [22] A. Kiejna, T. Ossowski, E. Wachowicz, *Surf Sci* **548** (2004) 22
- [23] P. Hohenberg, W. Kohn, *Phys Rev B* **136** (1964) 864
- [24] W. Kohn, L.J. Sham, *Phys Rev A* **140** (1965) 1133
- [25] M.C. Payne, M.P. Teter, D.C. Allan, T.A. Arias, J.D. Joannopoulos, *Rev Mod Phys* **64** (1992) 1045
- [26] W.E. Pickett, *Comput Phys Rep* **9** (1989) 115
- [27] E. Smargiassi, P.A. Madden, *Phys Rev B* **49** (1994) 5220
- [28] E. Smargiassi, P.A. Madden, *Phys Rev B* **51** (1995) 117
- [29] E. Smargiassi, P.A. Madden, *Phys Rev B* **51** (1995) 129
- [30] W. Kohn, L.J. Sham, *Phys Rev A* **140** (1965) 1133
- [31] D.M. Ceperly, B.J. Alder, *Phys Rev Lett* **45** (1980) 566
- [32] D.R. Hamann, *Phys Rev B* **40** (1989) 2980
- [33] N. Troullier, J.L. Martins, *Phys Rev B* **43** (1991) 1993
- [34] D. Vanderbilt, *Phys Rev B* **41** (1990) 7892
- [35] G. Kresse, J. Joubert, *Phys Rev B* **59** (1999) 1758

- [36] D.J. Chadi, M.L. Cohen, *Phys Rev B* **8** (1973) 5747
- [37] J.D. Joannopoulos, M.L. Cohen, *J Phys C* **6** (1973) 1572
- [38] H.J. Monkhorst, J.D. Pack, *Phys Rev B* **13** (1976) 5188
- [39] R.A. Evarestov, V.P. Smirnov, *Phys Status Solidi* **119** (1983) 9
- [40] R. Car, M. Parrinello, *Phys Rev Lett* **55** (1985) 2471
- [41] M. Born, J.R. Oppenheimer, *Ann Phys* **84** (1927) 457
- [42] J. Vandevondede, A. De Vita, *Phys Rev B* **60** (1999) 13241
- [43] M. Stengel, A. De Vita, *Phys Rev B* **62** (2000) 15283
- [44] A. Alavi, J. Kohanoff, M. Parrinello, D. Frenkel, *Phys Rev Lett* **73** (1994) 2599
- [45] N. Marzari, D. Vanderbilt, A. De Vita, M.C. Payne, *Phys Rev Lett* **82** (1999) 3296
- [46] F. Gygi, G. Galli, *Phys Rev B* **65** (2002) 220102
- [47] G. Kresse and J. Hafner, *Phys Rev B* **49** (1994) 14521
- [48] G. Kresse and J. Furthmuller, *Comp Mat Sci* **6** (1996) 15
- [49] G. Kresse and J. Furthmuller, *Phys Rev B* **54** (1996) 11169
- [50] J. Perdew, J. Chevary, S. Vosko, K. Jackson, M. Pederson, D. Singh, C. Fiolhais, *Phys Rev B* **46** (1992) 6671
- [51] P. Ziesche, S. Kurth, J.P. Perdew, *Comput Mat Sci* **11** (1998) 122
- [52] J.P. Perdew, K. Burke, M. Ernzerhof, *Phys Rev Lett* **77** (1996) 3865; **78** (1997) 1396 (E); **80** (1998) 891
- [53] Y. Zhang, W. Pan, W. Yang, *J Chem. Phys* **107** (1997) 7921
- [54] D.C. Patton, M.R. Pederson, *Phys Rev A* **56** (1997) R2495
- [55] D.C. Patton, D.V. Porezag, M.R. Pederson, *Phys Rev B* **55** (1997) 7454
- [56] J.P. Perdew, J.A. Chevary, S.H. Vosko, K.A. Jackson, M.R. Pederson, D.J. Singh, C. Fiolhais, *Phys Rev B* **48** (1993) 4978

- [57] V. Ozolins, M. Koerling, *Phys Rev B* **48** (1993) 18304
- [58] K. Momma, F. Izumi, *J Appl Crystallogr* **41** (2008) 653
- [59] J. Neugebauer, M. Scheffler, *Phys Rev B* **46** (1992) 16067
- [60] S. Nosé, *J Chem Phys* **81** (1984) 511
- [61] S. Nosé, *Mol Phys* **52** (1984) 255
- [62] P. Villars, *Pearson's Handbook: Crystallographic Data for Intermetallic Phases*, ASM International Desk Edition (1997)
- [63] D. Chen, Y.M. Wang, L. Chen, S. Liu, C.X. Ma, L.B. Wang, *Acta Mater* **52** (2004) 521
- [64] A. Kınacı, M.K. Aydınol, *Int J Hydrogen Energ* **32** (2007) 2466
- [65] B. Bogdanovic, K. Bohmhammel, B. Christ, A. Reiser, K. Schlichte, R. Vehlen, U. Wolf, *J Alloy Compd* **282** (1999) 84
- [66] B. Yazıcı, M.K. Aydınol, *Proceedings of International Hydrogen Energy Congress and Exhibition* (2005) Istanbul, Turkey
- [67] M. Tsuda, W.A. Diño, H. Kasai, H. Nakanishi, H. Aikawa, *Thin Solid Films* **509** (2006) 157
- [68] A.J. Du, S.C. Smith, X.D. Yao, G.Q. Lu, *J Phys Chem B* **110** (2006) 21417
- [69] A.J. Du, S.C. Smith, X.D. Yao, G.Q. Lu, *J Am Ceram Soc* **129** (2007) 10201
- [70] H. Smithson, C.A. Marianetti, D. Morgan, A. Van der Ven, A. Predith, G. Ceder, *Phys Rev B* **66** (2002) 144107
- [71] K.H.J. Buschow, P.C.P. Bouten, A.R. Miedema, *Rep Prog Phys* **45** (1982) 937